MPHIL

3D gene expression patterns, tissue anatomy and fate map of the developing chick wing

Downie, Helen

Award date:
2009

Awarding institution:
University of Bath

3D gene expression patterns, tissue anatomy and fate map of the developing chick wing

Helen Frances Downie

A thesis submitted for the degree of Master of Philosophy

University of Bath

Department of Biology & Biochemistry

February 2009

TABLE OF CONTENTS

Abstract

During vertebrate embryo development, patterning of the limbs is governed by the action of many genes. Here I have focused specifically on patterning of the digits and how they receive their identity (from thumb to little finger). I have used the chicken embryo as a model organism to study transcription factor-encoding gene expression patterns in the limb. I combined well described methods with a recently developed imaging technique, Optical Projection Tomography (OPT), to show analysis of these expression patterns in 3D. To investigate the eventual position of the descendants of cells of the early limb bud, I created a long-term fate map of the chick wing with use of the GFP-positive transgenic chicken. I have also analysed 3D images of known markers for the formation of skeletal structures in the limb and demonstrated how this could be combined with gene expression patterns and a comprehensive fate map in 3D to further understanding of limb development.

From creating a long-term fate map of the chick wing bud, I have established which areas of the early wing bud are the progenitors of each of the 3 digits of the forelimb. I have also shown how it would be possible to visualise this fate map in 3D and to combine this with 3D gene expression patterns of transcription factor-encoding genes known to be involved in digit patterning. Combining this information would show which genes are expressed in the digit progenitor cells through time, and may give an indication of the combination of genes that are required to give the digits their identity.

Table of Figures

List of Abbreviations

AP	Antero-posterior
BMP	Bone morphogenetic protein
DV	Dorso-ventral
GFP	Green fluorescent protein
HH	Hamburger & Hamilton
MABT	Maleic acid buffer + Tween-20
MRI	Magnetic Resonance Imaging
NTMT	NaCl, Tris, MgCl, Tween-20
OPT	Optical Projection Tomography
PBS	Phosphate buffered saline
PBT	Phosphate buffered saline + Tween-20
PD	Proximo-distal
Ptc	Patched
Shh	Sonic hedgehog
Smo	Smothened
TBST	Tris buffered saline + Tween-20
UV	Ultra violet
ZPA	Zone of Polarizing Activity

Acknowledgements

Most of all, I thank Cheryll for her guidance and hard work in helping me to carry out my project and in producing this thesis. Her enthusiasm and devotion has been extremely motivating throughout. I would also like to thank her for supporting me personally too and even coming to hear me playing my trumpet in the band!

My research was funded through grants from the Royal Society of London and from the Medical Research Council.

I thank everyone in our former lab at the University of Dundee, In particular Andy who taught me everything about OPT (and possible more). He has also been a continual support to us in Bath when we have had OPT problems and even by coming down to help us set everything up, so thanks Andy. Also helping me in Dundee was Malcolm who taught me all about Amira and other computer-related things. Some of the in situs and preliminary scans contributing to the results in Chapter 3 were carried out by Andy and Malcolm.

I would also like to thank past and present members of the lab in Bath. Specifically I'd like to thank Fiona for being patient and helping me with in situs and probe making, Matt for his help with cloning and for being good company through the long hours of "Graft Club". I also thank Laura for sharing the experience of relocating to Englandshire whilst remaining as Glaswegian as ever. I'm sure Twerton will miss us!

Many other people have helped make my time in Bath enjoyable; not least the members of Park Lane Big Band who let me join in and play a lot of fun gigs! I also thank my Mum and Dad and my brother, Tom for supporting me in everything I've chosen to do and for giving me good advice. Thanks also to Mike, just for being you.

Chapter 1: General Introduction

The mechanisms involved in patterning of the vertebrate limb are complex and intricate. During normal embryonic development, limbs emerge first as small buds from the body wall which elongate and widen through time and eventually the cells differentiate to form different types of tissue that constitute, for example, skeletal elements, muscle and connective tissue. There is a great amount of variation in the exact patterning of the limb between vertebrate species and even in the same animal, hindlimbs and forelimbs are patterned differently. These anatomical variations mirror the variety of specific uses and functions limbs have in vertebrates and have been shaped through evolutionary time.

Here I present findings that relate to our understanding of how the vertebrate limb is patterned along the antero-posterior axis (from thumb to little finger), and how these digits obtain their position and specific number of phalanges. My hypothesis here relates to whether the ultimate identity of a digit is determined by the combination of genes that are expressed in that digit's precursor cells.

For experimental purposes, I have used chicken embryos (*Gallus gallus*) as a model organism. Historically, chicken embryos have been used extensively in research and are useful for studying vertebrate embryo development for a number of reasons (Brown et al., 2003). Chickens, like all birds, are oviparous and so the embryo develops outside the mother's body, encased in an eggshell. This is extremely useful for developmental biologists because the embryo can be accessed easily, without damaging it or impairing its development, by simply making a small hole in the shell. This means that manipulations, such as grafting, can be made on the embryo, which can then be left to develop and the effect of the manipulation is observed later. In recent years, there has been a great increase in the availability of genetic resources associated with chicken

embryos. The chicken genome has been sequenced (Wallis et al., 2004) and Expressed Sequence Tag (EST) resources are available (ARK-Genomics), making genetic research more accessible.

Chicken embryos have been used specifically for studying limb development for many years for reasons outlined above but they are particularly suitable for this because each digit can be readily identified (See fig 1, C). The upper elements of the forelimb consist of a humerus, radius and ulna, much the same as in the human forearm but the hand consists of 3 digits rather than 5. These are named 2, 3 and 4 and have 2, 2 and 1 phalanges respectively.

1.1 AP Patterning of the limb

As mentioned, the limb grows out from the body wall first as a small bud. Its growth is governed by signals from the Apical Ectodermal Ridge (AER) (a thickened strip of ectoderm at the distal tip of the limb bud) and by the polarizing region (described below). The key signalling molecules of the AER are FGFs (Fibroblast Growth Factors). In fact the AER can be effectively replaced by FGF (Niswander et al., 1993). FGFs are effective in maintaining the polarizing region through a feedback loop with Sonic hedgehog (Shh) (Niswander et al., 1994, Laufer et al., 1994). Shh is the main signalling molecule controlling AP patterning.

1.1.1 The Zone of Polarizing Activity (ZPA)

Saunders and Gasseling discovered (1968) that if a particular piece of mesenchymal tissue at the posterior edge of the early chick limb bud was removed and transplanted into the anterior part of another chick wing bud, a complete extra set of digits would form in a mirror image of the normal pattern, so instead of the usual 234 digit pattern, a wing with 6 digits in a 432234 pattern formed. Signals from this part of the limb bud

were deemed to be responsible for the development and patterning of digits. It was later named the Zone of Polarizing Activity (ZPA) or the polarizing region. This discovery led to the creation of a classic model for the specification of digits (Tickle et al., 1975). By grafting a polarizing region at successive positions along the antero-posterior axis at the edge of the limb bud, it was apparent that the nature of each digit was determined by its distance from the nearest polarizing region. This could be explained if the polarizing region produced a morphogen, which diffused through the cells of the limb bud, and so the cells that were to become digits would experience different concentrations of the morphogen depending on their distance from the polarizing region. The polarizing activity of this region is conserved through vertebrate species as was discovered when polarizing region grafts from mouse embryos were transplanted into chick embryos where mirror image duplications resulted (Tickle et al., 1976).

1.1.2 The role of *Sonic hedgehog* in digit patterning

Sonic hedgehog (S*hh*) is a vertebrate gene related to the *Drosophila* segment polarity gene *Hedgehog*. It encodes a long-range signalling molecule that is effective in establishing polarity in a number of systems in development. The Shh signalling pathway involves two transmembrane proteins: Patched (Ptc) and Smoothened (Smo) (See supplementary figure 4 for an illustration of the pathway). Ptc1 is a receptor of Shh ligand (Marigo et al., 1996, Stone et al., 1996) and Smo is a signal transducer. In the absence of ligand, Ptc is required to inhibit the activity of Smo. In this case, Gli3 is cleaved it into a smaller protein (Gli3R), which acts as a transcriptional repressor of regulator genes and normally is expressed in a low to high gradient from anterior to posterior along this axis of the limb (Wang et al., 2000, Shin et al., 1999, Ruiz i Altaba, 1999). When Shh ligand is present, it binds to Ptc1 receptor proteins causing activation of Smo. This, in turn, allows the presence of Gli3 in the cell nucleus in its activator form.

[figure 1]

Figure 1. Chicken embryo and normal pattern of chick wing. OPT scans showing chick wings during development. (A) Volume rendering of 3D scan of whole chick embryo at stage 21 (Hamburger and Hamilton, 1951). Forelimb (FL) and hindlimb (HL) buds are indicated. (B) Digitally isolated right forelimb bud to demonstrate the axes of the limb: A = anterior, P = posterior, Pr = proximal, Dis = distal, D = dorsal and V = ventral. (C) OPT scan of wing at 10 days of development showing pattern of cartilage, stained using alcian green. Digits are indicated (2-4).

In the limb, *Shh* is expressed in the polarizing region and ectopic anterior expression of Shh causes digit duplications (Riddle et al., 1993). It is now known that the morphogen that leaves the polarizing region is based on Shh. In the absense of Shh, digits fail to develop. This is known from the phenotype of the chick mutant oligozeugodactyly (ozd) (Ros et al., 2003) where only the limbs develop lacking *Shh* expression posterior elements of the forelimb and hindlimb and are missing all digits other than digit 1 in the hindlimb. The mutation is thought to be a defect in a regulatory element which controls limb-specific expression of *Shh*. In the mouse mutant lacking Shh, no digits develop (Chiang et al., 1996).

Since the revelation of *Shh* involvement in digit patterning, there have been many studies concerning the exact nature of its role and regulation. As mentioned above, its expression is maintained via the Shh-Fgf feedback loop once it is initially activated by expression of *dHAND*, another transcription factor-encoding gene (Cohn, 2000).

Gli3 is involved in the development of digits. This is known because mutations resulting in over-expression of *Gli3* lead to phenotypes of extra digits (polydactyly). This link between Gli3 mutations and polydactyly has been described in relation to human congenital syndromes, for example, in Greig Cephalopolysyndactly Syndrome (Biesecker, 2008)

It is also clear that genes encoding bone morphogenetic proteins (Bmps) have an involvement in digit patterning as the extent of *Bmp* expression correlates with the digit character (Drossopoulou et al., 2000). 5' *Hoxd* gene products act at a transcriptional level as target genes of Shh signalling in digit patterning, although earlier 5' *Hoxd* genes are required for the onset of *Shh* expression (Tarchini et al., 2006).

It was found that in mouse, digits 4 and 5 are direct descendants of cells that expressed the *Shh* gene with some of the cells also contributing to digit 3. However, the specification of the remainder of digit 3 and all of digit 2 depend on a spatial gradient

of secreted Shh protein and digit 1 develops independently of Shh (Harfe et al., 2004). These findings led to the idea that the specification of digits depends on both a temporal gradient, relating directly to the expansion of the domain of descendants of *Shh* expressing cells, and a spatial gradient relating to cells receiving a degree of Shh protein depending on their distance from the expressing cells. In chick, this is not the case. From fate mapping experiments it has been postulated that the descendents of *Shh* expressing cells contribute only to more posterior elements (For example, Vargesson et al., 1997) but without the benefit of the ability to make a long-term fate map.

So it is now thought that Shh is effective in antero-posterior patterning of the limb through inducing growth of the digit forming field and through the establishment of a morphogen gradient, shown through experiments in chick where growth and Shh signalling were experimentally interrupted in the limb independently and together, resulting in different missing digits (Towers et al., 2008). Similar conclusions have been drawn from experiments in mouse (Zhu et al., 2008). A recent study used (ChIP)-on-chip analysis and transcriptional profiling of the mouse to create a picture of the genes involved in regulatory networks downstream of Shh signalling and therefore in digit patterning (Vokes et al., 2008). It is hoped that this will provide a framework of genes involved, giving an overall view of the pathway.

1.2 Application of 3D imaging in understanding embryonic development

There have been recent technological advances that have allowed for detailed 3D imaging of small tissue samples and therefore embryos. As much of the experimental evidence gathered from research in developmental biology is through visual observation, e.g. the study of phenotypes altered by manipulation or of gene expression patterns from *in situ* hybridisation experiments, it is only fitting that the methods used to create images have evolved to allow us to make more detailed analyses. Specifically, the ability to create images in 3 dimensions (3D) rather than 2D is an extremely powerful tool. Embryo development is an extremely dynamic 3D process and so visualising and recording data allows for building up a great deal of rich information which can be combined and analysed in a more detailed way.

μMRI is a form of the usual MRI (Magnetic Resonance Imaging), used in medicine to create images of the human body, which has been adapted in order to image much smaller specimens by employing stronger magnetic field gradients and external magnet. This allows for the production of a high resolution depending on the type of tissue to be imaged (Chudek et al., 1997). This technique has been utilized to create images of chick embryos where it is possible to identify internal organs and skeletal structures (Li et al., 2007). The same report presented data from images of live quail embryos *in ovo* and it also focused specifically on the anatomical structures of the chick wing at a stage where bone ossification is beginning to take place, and also later where individual muscles could be distinguished. A detailed 3D record of normal anatomical limb structures at various stages of development could prove extremely useful for comparison with limbs that have developed once manipulations have been made.

Here I have not used μMRI, but another recently developed imaging technique called Optical Projection Tomography (OPT) (Sharpe, 2002) which is useful as a tool for

studying embryos and for detecting colourometric staining (Sharpe et al., 2002). It can be used to generate images of a higher resolution than those created using μMRI for samples of up to 40mm in thickness. This technique can be used to detect transmitted light, projected through embryonic tissue, or emitted light from autofluorescence under ultra violet light. The data captured with transmitted light depends on optical density and thickness of tissue, and therefore is used to detect coloured staining. A series of images are captured as the sample is rotated through 360º which can then be reconstructed to form an accurate 3D image of the embryo. So the technique is un-invasive and also different wavelengths of light can be used for capturing different types of sample. Most usefully for the purpose of this thesis, is that it is possible to carry out a scan using fluorescent light to capture the form of the external surface and then a second scan of the same sample uses visible light to detect coloured staining from whole mount *in situ* hybridisation within the embryo. These two scans can then be assembled together to form images showing where the staining is present *in situ*, in 3D.

Various projects are currently using OPT as a device for imaging aspects of embryo development. Such projects as EMAP and EMAGE are underway at the MRC's Human Genetics Unit in Edinburgh (Baldock et al., 2003, Christiansen et al., 2006). These are projects aiming to create a digital atlas of gene expression and cell lineage data of mouse development. The information accumulated in this atlas has been gathered using a variety of imaging techniques, for example 2D pictures of whole mount *in situ* and section *in situ*. In collaboration with this overall project, an online resource has been released. It is an atlas specifically related to mouse limb anatomy and has been published as an online interactive 3D tool (Delaurier et al., 2008). OPT was used to gather the data for this project, which is hoped to be specifically useful for identifying phenotypes of transgenic mice by comparison with the 3D anatomy of the normal mouse limb.

Besides projects aiming to describe embryo anatomy in 3D, reports on gene expression patterns in 3D are also being produced using OPT. For example, there are now 3D

descriptions of *Wnt* and *Frizzled* gene expression patterns in the mouse embryo (Summerhurst et al., 2008). In chicken embryos, however, there have not been such advances, although there is a freely available online database of 2D Whole Mount *in situ* photographs, named GEISHA (Bell et al., 2004). This project and corresponding database has grown in size and become more comprehensive since it began. This highlights the demand for online references of gene expression to complement research in embryo development.

The results presented here will go towards a new project aiming to produce a database similar to the atlas that is being accumulated using mouse embryos. This atlas will comprise of 3D data of gene expression patterns and will employ OPT to generate the images. The establishment of this atlas will be extremely useful to developmental biologists as a queryable database where comparisons can be made between gene expression patterns and also between data from mouse and chick.

Recently, methods were defined and refined for utilizing new technologies to effectively compare gene expression patterns in the developing chick limb (Fisher et al., 2008). The novelty of this technique is combining the use of reference models of limb buds to align many expression patterns in the same space, allowing them to be compared effectively. I have employed these techniques here and have made use of the Bookstein thin plate spline algorithm (Bookstein, 1989) available with Amira® software. Similar gene mapping has been carried out using reference models where 3D data was generated by reconstructions of section *in situ* hybrization of the embryonic mouse brain (Lein et al., 2007). In the atlas project, once many patterns are accumulated and mapped to references, sophisticated data mining techniques can be applied which will allow us to analyse and compare the patterns computationally. This may lead to new associations for further study.

1.3 Aims of the current study

Here I aim to apply these techniques to compare expression patterns in the chick wing of genes involved in digit patterning. The genes have I have chosen have homologs in *Drosophila*, where they have an involvement in wing vein patterning (Biehs et al., 1998) and therefore are good candidates for being involved in the process of giving digits their identities.

I also aim to shown how this expression pattern data can be combined with data on tissue anatomy in 3D, which will allow for relating gene expression to limb morphogenesis. Examining tissue anatomy in the developing chick wing will provide a way of determining the extent of tissue specification at the stages I study.

My final aim is to produce a long-term fate map in 3D, firstly to determine, with certainty, which parts of the early limb bud are the progenitors of the digits. Secondly, this fate map could then be traced through various stages where I will also have data on gene expression patterns. This will allow me to observe which gene expressions digit progenitor cells are exposed to through development. It will then be possible to test whether it is these distinct combinations of gene expressions through time that give the digits their identity.

Chapter 2: General Materials and methods

This chapter details materials and methods used throughout. For materials and methods specific to grafting and use of the GFP chicken, see section 4.2.

2.1 Chicken embryos

Fertilized White Leghorn Chicken eggs from H. Stewart, Lincolnshire, were incubated at 37°C after being stored at 15°C for no more than one week. The eggs were incubated on their side, in a humidified incubator for the length of time required for the embryos to reach the appropriate Hamburger Hamilton stage (Hamburger and Hamilton, 1951).

2.2 Preparation of RNA probes for *in situ* hybridization

Plasmids containing the required genes are transformed into chemically competent *E. Coli* cells (One Shot® TOP10 cells, Invitrogen) by thawing the cells on ice for 15 minutes and then mixing in 1µl of plasmid stock. The mixture is left on ice for 30 minutes and then heat shocked at 42°C for between 45 and 60 seconds, after which it is put back on ice for 15 minutes. 80µl of Luria Broth is added to the cells, which are then shaken at 37°C for 40 minutes. The cells are then plated onto LB-Agar containing ampicillin (50µg/ml) and are grown overnight. The following day, a single colony is picked from each plate and used to inoculate 5ml LB with ampicillin. This is shaken overnight at 37°C.

DNA is isolated from the culture using a miniprep kit (Qiaprep spin miniprep kit 50, Qiagen). 15µl of plasmid DNA is linerised using 4µl of the appropriate enzyme, 10µl of the correct buffer and this is made to 100µl with dH_20. This mixture is left for at least 3 hours at 37°C, where a small sample is applied to 1% agarose gel with ethidium bromide, where the DNA fragments can be separated by electrophoresis to check that the DNA has been linerised and is of the correct size. The linerised DNA is then heated at 65°C for 20 minutes to inactivate the restriction enzyme. In some cases, phenol:chloroform extraction was carried out, as per Maniatis (1982), by making the DNA solution to 200µl with dH_20, adding 200µl of phenol:chloroform mix, shaking for 2 to 3 minutes then spinning in a centrifuge at 13,000rpm for 15 minutes. The DNA solution is removed by taking the top layer of liquid, which is then added to a fresh tube with 200µl chloroform. This is then shaken and spun as above.

The DNA solution is always precipitated with ethanol (2.5 x volume of DNA solution) and 3M sodium acetate (0.1 x volume of DNA solution). These are added to the DNA solution and left at -20°C for 30 minutes, after which the solution is spun at 13,000rpm at 4°C for 30 minutes, washed with 70% ethanol and spun for 5 minutes at 13,000rpm. The 70% ethanol is then removed and the tube is left to air dry for around 20 minutes. The DNA is re-suspended in 20µl dH_20. At this stage the DNA content of the sample is checked using electrophoresis as described above.

The RNA probe is synthesised using 1µl of the linerised, precipitated plasmid, 1µl of the appropriate RNA polymerase, 0.5µl of RNAse inhibitor (Roche), 2µl DIG RNA labelling mix (Roche), 2µl DTT, 4µl 5X transcription buffer, and 9.5µl dH_20. This mixture is left at 37°C for at least 2 hours. The mixture is then made to 50µl with dH_20 for purification using a spin column (Illustra probe quant G-50 micro column, GE Healthcare). A small volume is run on a 1% agarose gel with ethidium bromide to asses the concentration of RNA. All of the remaining product from the column is diluted in 10ml of hybridization buffer and stored at -20°C for use in whole mount *in situ* hybridization experiments.

Probes were made using the following restriction enzymes and RNA polymerase:

Gene name	Restriction Enzyme	RNA polymerase	Reference
Tbx2	Nco1	T7	(Logan et al., 1998)
Tbx3	Xho1	T3	
Csal1	HindIII	T7	(Sweetman et al., 2005)
Hoxd13	EcoRV	T3	(Zakany et al., 2004)
GFP	PCR used	Sp6	[See section 4.2]

2.3 Whole Mount RNA *in situ* hybridization

2.3.1 Embryo fixation

The eggs are windowed and, the following day, dissected by removing the embryo from the egg into cooled PBS where the membranes are removed. I used embryos between the HH stages 21 and 27. The head and heart are removed to prevent interference from strong signals when scanning. The embryo is then transferred into 4% paraformaldehyde for fixation overnight at 4°C. After fixation, embryos are dehydrated through a series of methanol concentrations in PBS (25%, 50%, 75% and 100%). At this point the embryos can be stored in 100% methanol for up to one month at -20°C.

2.3.2 Prehybridization

Embryos are rehydrated through a series of methanol concentrations in PBS (75%, 50% and 25%) for 5 minutes at each concentration followed by two 10 minute washes in PBT. The embryos are then permeabilized using proteinase K diluted in PBS (10µl/ml)

for 30 seconds per HH stage (e.g. 12 minutes for stage 24 embryos). This is followed by three quick washes in PBT, after which the embryos are fixed in 4% PFA, 0.1% gluteraldehyde at 4°C for 20 minutes. The embryos are then washed 4 times for 5 minutes in PBT, followed by prehybridization at 65°C by leaving the embryos in hybridization buffer until they sink, changing the solution and leaving for 3 hours.

2.3.3 Detection of RNA transcript

The prehybridization buffer is replaced by pre-warmed DIG-labelled RNA probe in hybridization buffer (50µl probe in 10ml buffer), which is usually left overnight at 65°C but can be left for up to 3 days to allow the RNA probe to hybridize. After hybridization, the embryos are washed as follows: once in fresh hybridization buffer for 30 minutes at 65°C, 2 washes in 2xSSC (See appendix 2) for 10 minutes, 3 20 minute washes in 2xSSC/0.1% CHAPS (3-[(3-Cholamidopropyl)dimethylammonio]-propanesulphonate) (Fisher), 3 20 minute washes in 0.2%SSC/0.1% CHAPS, each at 65°C. The embryos are then washed twice in MABT (see appendix 2) at room temperature for 10 minutes followed by a 3 hour wash in 3% blocking reagent (Roche) which helps to reduce background detection. The embryos are then washed overnight at 4°C in anti-DIG antibody conjugated with alkaline phosphatase (Roche) at a concentration of 1:1000 in 3% blocking buffer in MABT as above. The embryos are then put through 5 one hour washes in MABT at room temperature, and left overnight in MABT at 4°C to remove any residual antibody. Then, to detect the alkaline phosphatase, the embryos are transferred into glass bijous and washed twice for 20 minutes in freshly made NTMT at room temperature. The colour reaction is started by adding 2.5µl NBT (nitro blue tetrazolium) (Sigma) and 2.5µl BCIP (5-bromo-4-chloro-3-indolyl phosphate) (Sigma) per ml NTMT. The detection is allowed to occur in the dark until an appropriate colour reaction has occurred. At this point the reaction is stopped by replacing the NTMT with 4% formal saline fixative.

2.3.4 Extra washes for embryos to be scanned using OPT

Embryos, after whole mount RNA *in situ* hybridization, that are to be scanned using OPT go through extra washes to ensure that there is no residual NBT/BCIP which may cause interference during OPT scanning. After fixation overnight in 4% formal saline, the embryos go through the following washes at room temperature: 2 x 10 minute washes in PBS, 1 x 5 minute wash in 10xTBST (see appendix 2) (or until the embryo sinks), 3 x 20 minutes in 1xTBST. Then the embryos are placed in 1xTBST at 4°C. The following day, the embryos are washed 3 times for 5 minutes in PBS at room temperature and then fixed overnight in 4%PFA at 4°C. This extra fixation step helps to prevent leaching out of the signal during later steps in the preparation towards scanning. The embryos are given 2 quick washes in PBS and then are fixed in 4% formal saline. At this stage, embryos can be stored at 4°C.

2.4 Optical Projection Tomography

2.4.1 Embedding and block cutting for OPT

Before embedding, embryos are given 2 10 minutes washes is PBS. In some cases, a high magnification scan is required where the embryos were dissected such that only the trunk with right and left wing buds was scanned. They are dissected using a fresh razor blade. 1% low melting point agarose in water is prepared by microwaving, leaving to cool in a 55°C water bath and then filtering through a standard 500ml 0.45µm membrane filter using a vacuum pump.

The agarose is poured into a 50mm high-wall petri dish where it starts to cool surrounded by ice in a large petri dish. The temperature is allowed to drop to approximately 30°C, and the dissected embryos are placed into the agarose (2 per dish). Blunted and hooked short glass pipettes are used to manoeuvre the embryos so they are suspended midway between the agarose meniscus and the base of the dish, parallel to the base, as the agarose is cooling and beginning to solidify. When the embryo is in the appropriate position, the dishes are left at 4°C for at least an hour.

A block of agarose with 8 sloped sides containing the embryo is required to carry out each scan. To do this, the agarose containing the embryos is removed from the petri dish. Now that the agarose has solidified, it is possible to slice it using a fresh single-edge razor blade. A hexagonal block of agarose is produced, with the embryo in the centre of this block with its midline perpendicular to the base of the block and its limb buds parallel to the base of the block.

Once the block has been cut, it is placed in a small glass jar and dehydrated through a series of methanol concentrations (10%, 25%, 50%, 75%, and 100% in dH_2O). Each dehydration step lasts at least 1 hour and the 100% methanol step is carried out twice.

Before scanning, the samples are cleared in BABB (benzyl alcohol: benzyl benzoate both from Sigma), 1:2). The samples are normally left in BABB overnight before scanning. The samples are glue to a metal mount prior to scanning.

2.4.2 Scanning and reconstruction

Scans are carried out using a prototype OPT machine created at the HGU-MRC in Edinburgh with its associated software, also created at the HGU-MRC. 400 images are captured using a Leica MZ 16FA microscope and Q Imaging, Retiga Exi camera, while the sample is rotated through 360°. Each embryo is scanned twice – once using the fluorescence channel to visualise tissue from autofluorescence emission. The second scan uses the bright field channel with a 700nm filter. This scan detects NBT/BCIP staining. The output from these scans is an image, which can then be reconstructed using the program MAPaint, generated at HGU-MRC. After the reconstruction process, the end product is a 3D object which can be viewed through 3 sets of tiff stacks for each scan. The data can be uploaded to the Amira® software package for further visualisation and mapping.

2.4.3 Visualisation and mapping of 3D data

In order to visualise the images of scanned embryos, Amira©, the 3D modelling and visualisation program commercially available from Visage Imaging™, is used. Likewise, this software is used to compile scanned data of 3D gene expression patterns onto a reference limb. The limb of the embryo showing gene expression is digitally isolated and, if necessary, scaled up or down to be at the same scale as the reference model. It is then moved to overlap with the reference model as closely as possible before landmarks are defined which match the external anatomy of the limb of the embryo that has been scanned with the reference limb of the same stage. Very accurate stage matching is extremely important to allow effective mapping. Depending on the stage of the limb bud, between 40 and 100 landmarks are specified. Once the

landmarks are in place, the anatomy of the limb from the fluorescence scan is warped to the reference using the Bookstein thin plate spline algorithm (Bookstein, 1989) available with Amira® software. If the allocation of landmarks and warping were effective, this warped limb should be almost identical to and occupy the same space as the reference limb. Only when this is the case, the same warp is applied to the bright field scan showing the gene expression pattern.

2.4.4 Creation of median 3D pattern

It was found that the most suitable way of creating an accurate 3D expression pattern was to use at least three individual scans of the same expression pattern at the same stage, which are each mapped to the reference model as described above. Then a median can be calculated (Fisher et al., 2008). This is done using programs generated in-house at the MRC HGU, Edinburgh. The data from the warped scans are converted into the "Woolz (Wlz)" file format, which is specific to software produced at the MRC HGU.

Once they have been converted, the files can then be used to produce a median dataset using the Wlz-based program "WlzFilterNObjsValues". This program works by reading the domains of all the expression patterns and making a reference domain which is the union of all the input domains. It then takes the grey level values for each point in the input data and calculates a ranked value of the grey values across all of the expression patterns. The middle rank corresponds to the median.

2.4.5 Making movies

Once the median expression patterns have been generated and a number of different patterns accumulated onto a reference, movies are made to allow for better appreciation of the 3D images. This is done using the "MovieMaker" function of Amira®.

2.4.6 Measurement of volumes

Measuring the volume of the limb buds and of expression patterns is carried out using Amira®. The "LabelVoxel" module is used to create a domain representing the volume to be measured, using the same threshold as used to visualise the object. At this point, the "TissueStatistics" module and "Measure" can be used can be used to calculate the volume.

To measure the overlap of two expression patterns, the "arithmetic" module is used to create produce a domain of only the overlap and the volume of this can be calculated as described above. This data can then be used to calculate the percentage of overlap between expression patterns and the percentage of the limb bud with expression.

Chapter 3: Selection of expression patterns of genes encoding transcription factors in chick limb development.

3.1 Introduction

3.1.1 Transcription factor-encoding genes involved in digit patterning.

I have investigated the expression patterns of various transcription factor-encoding genes in the chick wing in detail at three different stages of embryonic development. In particular, I have studied the expression patterns of the genes *Tbx2*, *Tbx3*, *Csal1*, *Csal3* and *Hoxd13* at stages 21, 24 and 27. I have chosen these stages based on the different properties of the limb bud has through these stages. Summerbell reported (1974) that by carrying out a ZPA graft into a stage 21 host embryo, it is possible to create a full mirror image duplication of the elements of the hand, whereas by carrying out the same procedure on a stage 24 wing bud, it is only possible to create duplications of the very distal elements of the digits. So, there is a clear difference in the degree of specification of the eventual skeletal pattern of the limb between these stages and it is possible to conclude that by stage 24, the digits have begun to become specified. By stage 27, the skeletal elements of the wing bud are beginning to be laid down in cartilage, as described later. Therefore this stage represents another distinct phase of limb development where analysis of gene expression patterns could provide useful insights into the developmental mechanisms.

The transcription factor-encoding genes I have investigated have homologs in *Drosophila* where they are known to have a function in the patterning and development

of wing veins. In *Drosophila* development, the wings emerge from imaginal discs where it is thought that a vein-specific genetic programme at this stage governs the later patterning of wing veins (Biehs et al., 1998). This genetic programme leads to the formation of boundaries along the A-P axis between domains of gene expression patterns. These boundaries may delineate stripes where the vein will form, intervein stripes or broader domains encompassing an area where veins will form. I have applied this concept to the development of vertebrate limbs where the veins are represented by digits. It is possible that in the development of vertebrate limbs, there is a code of transcription factor-encoding genes expressed in the limb bud prior to the formation of digits, which results in their correct A-P patterning.

3.1.2 *T-box* genes

T-box proteins are characterised by a DNA binding site, which is highly conserved through vertebrate and invertebrate species. In *Drosophila*, the *Optomoter-blind* (*Omb*) gene shares this conserved region, called the T-box (Pflugfelder et al., 1992). *Omb* has a role in fly wing development, where it has been shown to stabilise the A-P boundary of cells, thereby preventing the formation of folds or clefts in the wing (Shen et al., 2008). I have focused on the expression patterns of two T-box genes known to be involved in vertebrate limb development; *Tbx2* and *Tbx3*. These genes are closely related members of the T-box family of genes and share similar expression patterns in the hindlimb and forelimb, consisting of an anterior and posterior stripe (Isaac et al., 1998, Gibson-Brown et al., 1998, Logan et al., 1998). This was thought to be achieved through BMP and Shh signalling (Suzuki et al., 2004), another parallel with the control of *Omb* in *Drosophila,* which is achieved through signalling by Hedgehog and Decapentaplegic, the respective relatives of vertebrate Shh and BMP (Tumpel et al., 2002). Although *Tbx2* may be a candidate for acting upstream of *Shh* and restricting its expression to the posterior margin of the limb bud (Nissim et al., 2007).

It has been reported that there are differences between the mechanisms regulating the posterior and anterior stripes of *Tbx3* expression in the limb bud. The posterior stripe is stable and depends on the Shh signalling cascade, whereas the anterior stripe is negatively regulated by Shh and depends on anterior BMP signalling (Tumpel et al., 2002). Because expression of *Tbx2* and *Tbx3* occurs with such sharp boundaries towards the middle of the limb bud, there may be other inhibitory factors being expressed here.

In humans, spontaneous mutations in *Tbx3* can be responsible for the congenital disorder Ulnar-mammary syndrome (Bamshad et al., 1999, Bamshad et al., 1997). This disorder manifests itself through craniofacial, mammary tissue, apocrine, urogenital and forelimb abnormalities. The forearm defects can consist of a complete loss of posterior

digits and the ulna. These defects have also been demonstrated in homozygous mouse mutants (Davenport et al., 2003). Both *Tbx2* and *Tbx3* are required for the specification and formation of posterior digits.

3.1.3 *Spalt* genes

The *Spalt* genes encode proteins that have a zinc finger DNA binding domain. They are highly conserved through many vertebrate and invertebrate species where they have important roles in the development and patterning of multiple organ systems. The zinc finger-encoding region of the gene is the most homologous and part of the sequence, conserved through various species(Barrio, 1996). In humans, mutations in the gene *Sall1* can cause Townes-Brocks Syndrome (TBS) (Kohlhase et al., 1998). TBS presents with various physical abnormalities including preaxial polydactyly. This disorder has been replicated using mouse mutants where the heterozygous mutant shows defects mimicking those present in TBS, including wrist bone deformities (Kiefer et al., 2003).

There are two closely related *Spalt* genes described in *Drosophila*, *Spalt major* (*salm)* and *Spalt related* (*salr*), which broadly regulate patterning and cell fate (Chen et al., 1998). They share very similar expression patterns in the wing disc and are both involved in wing vein patterning in that their expression boundary in the imaginal wing disc corresponds to the LII and LV longitudinal wing vein primordium (Barrio, 1996). Disrupting the expression pattern of *Salm* causes the LII wing vein to develop abnormally and to form branches (Sturtevant et al., 1997). Another study determining the functional significance of *Salm* and *Salr* in *Drosphila* used mosaic wings with mitotic clones to remove both genes and found that in addition to the disruption of wing vein patterning, the wing size was affected. Therefore these genes may be required for proper wing growth in *Drosophila* development (de Celis et al., 1996). It has been shown in Medaka that *Spalt* is a direct target of the Hedgehog signalling pathway (Koster et al., 1997), and this is probably true in chick although this has been

demonstrated more indirectly. *Csal1* expression has been shown to respond to both FGF and Wnt signalling (Farrell and Munsterberg, 2000), both which play roles in maintaining *Shh* expression. Therefore, Shh signalling is also likely to be involved in the regulation of *Csal1*.

I have focussed on the expression patterns of *Csal1*, most closely related to *Sall1* in humans, and *Csal3*, which is closely related to *Sall3* in humans. It is not clear which *Drosophila Spalt* genes these are most closely related to. It may be the case that a common ancestor of vertebrates and invertebrates had only one *Spalt* gene, which later diverged to form the two *Spalt* genes now present (de Celis et al., 1996). The proteins transcribed by these genes physically interact with one another and their DNA binding capabilities indicate that they may be transcriptional regulators (Sweetman et al., 2003). It has been suggested that the non-DNA-binding part of the protein has a greater degree of sequence variation through different species and may be involved in determining protein-protein interactions (Barrio, 1996). Given these considerations along with the interesting expression patterns of *Spalt* genes in the developing wing bud, I have studied the dynamics of these patterns in detail.

3.1.4 *Hoxd13*

The *Hox* genes are another family of transcription factor-encoding genes that are highly conserved throughout all metazoans. They share part of their sequence, known as the homeobox and broadly, they act as determinants of regional identity in development. They were first discovered in *Drosophila* in 1915 (Bridges and Morgan, 1923), where the *Hox* genes include *Bithorax* (*bx*) and *Antennapaedia* (*Ant*). Gain of function studies in these genes have shown that *Hox* genes act as determinants of regional identity (Graham et al., 1989). In mammals, there are clusters of *Hox* genes found on four chromosomes. These clusters are named A, B, C and D and in limb development, the most prominently expressed *Hox* genes are of the 5' regions of the *Hoxa* and *Hoxd* clusters (Wellik and Capecchi, 2003). These gene clusters exhibit spatial and temporal

co-linearity where the 3' genes are expressed prior to and more proximally than 5' genes. In early patterning of the limb, *Hox* genes play an important role in determining the localized posterior expression of *Shh* allowing correct A-P patterning to take place (Zakany et al., 2004).

Hoxd13 is the last vertebrate *Hox* Gene to be expressed. In the developing limb bud it acts as a marker of cells that will form the digit plate (Zakany et al., 2004). In mice, the disruption of *Hoxd13* via homologous recombination in embryonic stem cells caused limb defects such as reduction in length of skeletal elements, loss of phalanges and bone fusions (Dolle et al., 1993). Later, it was found through making mice with combinations of mutations in the *Hoxa13* and *Hoxd13* genes that these two genes act in a partially redundant manner where single heterozygous mutations show compensation phenotypes (Fromental-Ramain et al., 1996). *Hoxa13/Hoxd13* compund heterozygotes display phenotypes observed in *Hoxd13* null mutants (Dolle et al., 1993).

3.2 Results

3.2.1 Stage 21

Tbx2 and *Tbx3* expression patterns are similar and occur in two distinct stripes: one in the anterior and one in the posterior of the limb (Isaac et al., 1998, Gibson-Brown et al., 1998, Logan et al., 1998). At this stage, the stripes do not extend to the distal tip (Fig. 3.1, C.iv). By visualising the expression patterns of these genes in 3D, I show that in the posterior of the limb, *Tbx2* expression occurs entirely within the expression domain of *Tbx3* (Fig. 3.1, C.ii). However, in the anterior stripe, the inverse is true, and expression of *Tbx3* is entirely overlapped by *Tbx2* expression. Particularly in the posterior stripe, it is noticeable that the expression is not uniform across the dorso-ventral axis, but instead forms a cup shape with an area of non-expression in the centre (indicated by white arrow, Fig. 3.1, C.ii). Although there are slight differences in the shapes of the expression patterns of these T-box genes, it is important to note that they are very similar. It is possible to quantify the volume of these expression patterns as a percentage of the wing bud (Fig. 3.2, A). The majority of each of these expression patterns occurs in an overlapping space within the wing bud at this stage: specifically, 68% of *Tbx2* expression overlaps with *Tbx3* expression and 82% of *Tbx3* expression overlaps with *Tbx2* expression.

Figure 3.1, E shows the expression pattern of *Csal1*. There is a single domain of *Csal1* expression in the limb, which is posterior and distal at stage 21. The expression pattern is quite symmetrical across the dorso-ventral axis. At this stage, there is no expression of the *Spalt* gene *Csal3*. *Hoxd13* expression is shown in Fig 3.1,D and F. This pattern is also posterior and distal at this stage, although the region of expression is smaller than that of *Csal1*. Unlike *Csal1* expression, *Hoxd13* expression is asymmetrical across the dorso-ventral axis with more expression in the dorsal region (Fig 3.1, D). Comparison of these two expression patterns shows that *Hoxd13* expression is almost entirely within the domain of *Csal1* expression at this stage (Fig 3.1, F). There is only a small dorsal region of *Hoxd13* expressing cells not expressing *Csal1* (white arrows,

Fig. 3.1, F). This region is equivalent to 21% of the entire *Hoxd13* domain (Fig. 3.2, B).

[Figure 3.1]

Figure 3.1. Comparison of 3D gene expression patterns in the stage 21 wing bud. (A-C) Dorsal views of 3D isosurface representations of a stage 21 wing bud with expression patterns of *Tbx2* (A), *Tbx3* (B) and both *Tbx2* and *Tbx3* shown together (C). Orange lines represent the positions of the sections shown in Cii and Ciii. (Cii-Civ) 2D virtual sections of limb bud showing *Tbx2* and *Tbx3* expression where overlapping regions are shown in white, *Tbx2* alone in green and *Tbx3* alone in pink. (Civ) Section taken through plane of the paper. A = anterior, P = posterior, D = dorsal, V = ventral, Pr = proximal, Di = distal. (D-F) Dorsal views of same wing bud showing expression patterns of *Hoxd13* (D), *Csal1* (E), and *Hoxd13* and *Csal1* together with the overlapping region in white (F). Sections are shown in the same orientation as Cii, and the orange lines indicate the section position along the proximo-distal axis.

[Figure 3.2]

Figure 3.2. Graphs quantifying pair-wise comparisons of gene expression patterns in the stage 21 wing bud. (A) Comparison of volume of expression patterns of *Tbx2* and *Tbx3* measured as a percentage of the entire limb bud. The white regions of the bars show the proportion of the total expression volume that overlaps with the expression of the other gene shown on the graph. The coloured parts of each bar represent the regions of respective *Tbx2* (turquoise) and *Tbx3* (pink) expression that do not overlap with one another. Numbers shown on the bars indicate the proportions of overlapping and non-overlapping regions. (B) Comparison of *Csal1* (red) and *Hoxd13* (purple) expression, using same format as (A).

3.2.2 Stage 24

Tbx2 and *Tbx3* are shown separately and overlapping (Fig. 3.3, A-C). By this stage, both of these genes are known to display asymmetry in the levels of expression in the posterior and anterior stripes where the anterior stripes do not extend as far distally or towards the centre of the limb bud as the posterior stripes (Gibson-Brown et al., 1998). I have shown, in section, the areas where the expression patterns of these genes overlap (Fig 3.3, Cii-iv). *Tbx3* expression is almost entirely overlapped by *Tbx2* expression and there are also regions of the limb bud expressing *Tbx2* alone. This is true of both anterior and posterior areas of expression. These observations are confirmed by quantifying the volumes of expression and overlap (Fig. 3.4, A). 71% of *Tbx3* expression occurs in the same domain as *Tbx2* expression, whereas this overlapping region represents only 29% of the total *Tbx2* expression at this stage. This difference in the expression domains of *Tbx2* and *Tbx3* is mostly due to differences in the expression through the dorso-ventral axis between these genes. The posterior area of expression of *Tbx3* forms a cup shape through this axis, similar to the pattern observed at stage 21. However this is not the case for *Tbx2*, which is expressed in a more uniform way.

Csal1 transcripts, at this stage, are spread across the posterior and distal parts of the limb. Virtual sections through distal region of the limb show that the expression spreads almost completely along the A-P axis (Fig. 3.3, E.ii). *Hoxd13* expression is also posterior and distal at this stage but does not reach as far towards the anterior of the limb as *Csal1*. At this stage, *Hoxd13* expression is not dorsally restricted, as observed at stage 21. Fig. 3.4, B shows that the overlapping region of *Hoxd13* and *Csal1* expression represents 61% of the total volume of *Csal1* expression and 84% of the total volume of *Hoxd13* expression.

The transcription factor-encoding gene *Csal3* is also expressed by this stage, although not at the earlier stage considered. It has a striking expression pattern that, from a

dorsal view, seems to be in a posterior, distal position in the limb. However, viewed in transverse section (Fig 3.3, F.ii), I observe that it is also dorsally restricted and forms a curved shape. As mentioned above, the proteins encoded by these spalt family genes, *Csal1* and *Csal3*, have been shown to interact with one another (Sweetman et al., 2003). Although the functional significance of this interaction is not fully understood, it is interesting that they are expressed in similar domains. At this stage, 72% of the *Csal3* expressing region also expresses *Csal1*. In the section showing both patterns, *Csal3* is entirely within the domain of *Csal1* expression (Fig. 3.3, H.ii), but it is also evident that there is an anterior ventral domain with *Csal1* expression alone.

[figure 3.3]

Figure 3.3. Comparison of 3D gene expression patterns in the stage 24 limb bud. (A-C) Dorsal views of 3D isosurface representations of a stage 24 wing bud with expression patterns of *Tbx2* (A), *Tbx3* (B) and both *Tbx2* and *Tbx3* shown together (C). Orange lines represent the positions of the sections shown in Cii and Ciii. (Cii-Civ) 2D virtual sections of limb bud showing *Tbx2* and *Tbx3* expression where overlapping regions are shown in white, *Tbx2* alone in green and *Tbx3* alone in pink. (D-F) Dorsal views (i) and virtual sections (ii) of a limb bud showing expression patterns of *Hoxd13* (D), *Csal1* (E), and *Csal3* (F). (G&H) Pair-wise comparisons of *Csal1* and *Hoxd13* (G) and *Csal1* and *Csal3* (H) as dorsal views (i) and as virtual sections where overlapping regions are shown in white (ii).

[Figure 3.4]

Figure 3.4. Graphs quantifying pair-wise comparisons of gene expression patterns in the stage 24 wing bud. (A) Comparison of volume of expression patterns of *Tbx2* and *Tbx3* measured as a percentage of the entire limb bud. The white regions of the bars show the proportion of the total expression volume that overlaps with the other gene expression shown on the graph. The coloured parts of each bar represent the regions of respective *Tbx2* and *Tbx3* expression that do not overlap with one another. Numbers shown on the bars indicate the proportions of overlapping and non-overlapping regions. (B) Comparison of *Csal1* and *Hoxd13* expression in same format as (A). (C) Comparison of *Csal1* and *Csal3* expression, again in the same format.

3.2.3 Stage 27

Tbx2 and *Tbx3* continue to be expressed at stage 27, where their expression patterns remain as anterior and posterior stripes. By observing these expression patterns in 3D at this stage, I show not only that the *Tbx3* expression domain extends further from the anterior and posterior margins than *Tbx2*, but it also extends further distally and retains a cup shape in the dorso-ventral axis, which was also observed at stage 24. *Tbx2* is not expressed in a cup shape like this, but it does appear to show a ventral skewing (Fig 3.5, Ci&ii). So by this stage, the extent of each pattern has changed. I have quantified the comparison between *Tbx2* and *Tbx3* in Figure 3.6, which shows that 64% of *Tbx2* expression shares its domain of expression with *Tbx3* but this represents 45% of the total volume of *Tbx3* expression. So, in fact, a substantial amount of *Tbx3* expression at this stage occurs out-with the domain of *Tbx2*.

Here, *Hoxd13* remains to be expressed distally and viewed in section, appears to be ubiquitous through both dorso-ventral and antero-posterior axes. In comparison with its expression at stage 24, it seems to have spread further anteriorly. This is due to the way in which growth occurs in the wing bud. Fate mapping experiments have shown that the posterior part of the early limb bud expands much more than the anterior part, giving rise to the distal part of the limb at later stages (Vargesson et al., 1997).

The *Spalt* family genes, *Csal1* and *Csal3* show intriguing expression patterns at this stage. *Csal1* expression has shifted away from the distal tip of the limb bud and now appears fairly centrally in the limb (Fig. 3.5, E). Unlike at previous stages of development, *Csal1* is now expressed in a dissimilar domain to *Hoxd13*. Figure 3.6, B. shows that only 16% of *Hoxd13* expression overlaps with that of *Csal1*. In terms of the A-P axis, *Csal1* is also fairly central, not extending to the anterior or posterior border of the wing bud. From a dorso-ventral point of view, the expression does spread between the dorsal and ventral surfaces but with more weight towards the dorsal side.

[figure 3.5]

Figure 3.5. Comparison of 3D gene expression patterns in the stage 27 limb bud. (A-C) Expression patterns of *Tbx2* (A) and *Tbx3* (B) and both patterns together (C). (Cii-iv) Virtual sections of Ci where the positions of the sections are indicated by corresponding orange lines. Sections are shown in same orientation as in Figures 3.1 and 3.3, although sections are shown at 2 positions along the proximo-distal axis and no section through plane of paper is shown because of the curvature of the wing bud at this stage. (D-F) *Hoxd13, Csal1,* and *Csal3* expression patterns shown as dorsal views (i) and as virtual sections (ii). (G-I) Comparisons of *Csal1* and *Hoxd13*, *Csal1* and *Csal3*,*Tbx3*and *Csal1, Tbx3* and *Csal13*, respectively. Shown as dorsal views and as virtual sections.

[Figure 3.6]

Figure 3.6. Graphs quantifying pair-wise comparisons of gene expression patterns in the stage 27 wing bud. (A) Comparison of volume of expression patterns of *Tbx2* and *Tbx3* measured as a percentage of the entire limb bud. The white regions of the bars show the proportion of the total expression volume that overlaps with the other gene expression shown on the graph. The coloured parts of each bar represent the regions of respective *Tbx2* and *Tbx3* expression that do not overlap with one another. Numbers shown on the bars indicate the proportions of overlapping and non-overlapping regions. (B-E) Comparison of volume of expression and overlap of *Csal1* and *Hoxd13* (B), *Csal1* and *Csal3* (C), *Csal1* and *Tbx3* (D), and *Csal3* and *Tbx3* (E), all using the same format as (A).

In contrast to the previous stage studied, the expression of *Csal3* is quite different to that of *Csal1*. In fact, they are now almost complementary. In the proximo-distal axis, it occurs at around a similar position as *Csal1* but this is about the extent of their similarities. *Csal3* shows only a small region of expression in the posterior margin of the wing bud and by studying the dorso-ventral expression, the clear cup-shape, hugging the ectodermal surface of the limb, becomes apparent. Comparing these expression patterns in section, *Csal1* expression is almost nestled in the cup shape of *Csal3* expression, with only small regions of overlap in the most anterior regions of *Csal3* expression. There is also a notable difference in the volume of their expression patterns: *Csal1* expression amounts to 9.27% of the entire volume of the limb bud, whereas only 2.4% of the limb bud is occupied by *Csal3* expression.

I have also made a comparison between *Csal1* and *Tbx3* expression (Fig. 3.5 Ii & ii). It seems quite striking the way in which *Csal1* expression sits neatly inside the cup shape of *Tbx3* expression with no overlap. This finding highlights the advantage of imaging in 3D, because from a view of the dorsal surface alone, it would seem that these two patterns do overlap when in fact they do not. The posterior stripe of *Tbx3* expression and *Csal3* expression at this stage seem to share this cup shape feature and 73% of *Csal3* expression is overlapped by the posterior stripe of *Tbx3* (Fig 3.5, Iiii).

3.3 Discussion

Detailed examination of the expression patterns of these transcription factor-encoding genes in the developing chick wing bud allows for great appreciation of their dynamic nature through the time course of early development. Further appreciation of the 3D images can be made from the animated movies on the attached CD-Rom. See Appendix 1 for descriptions of the movies.

3.3.1 *T-box* genes

Various shifts in the expression and relationship of expression patterns between *Tbx2* and *Tbx3* expression occur through the three stages of development that I have investigated. By stage 21, both *Tbx2* and *Tbx3* are expressed in patterns showing a cup-shape through the dorso-ventral axis and, also through this axis, *Tbx2* shows a slight ventral skewing whereas *Tbx3* does not. By stage 24, *Tbx2* expression has lost this cup-shaped pattern in the D-V axis and shows a slight ventral skewing only in the anterior stripe. At this stage, *Tbx3* expression has retained this cup-shape and still does not show any notable D-V bias. By stage 27, *Tbx2* is still not expressed in a cup-shape but shows a greater degree of ventral skewing than at the previous stage. *Tbx3*, however, remains expressed in a cup-shape and is ventrally skewed in the anterior stripe. The other notable change at this stage is that the posterior stripe of *Tbx3* expression extends to the distal tip of the limb bud whereas the posterior stripe of *Tbx2* expression is more proximally restricted.

By analysing graphs that quantify the expression and relationship of these genes (Fig, 3.2, 3.4 and 3.6), it is possible to make further observations on their changing expression patterns. I have also collated these data from all three stages and compiled a line graph to show the change in volume of expression through these stages (Fig 3.7). From this it is possible to deduce that *Tbx3* shows a substantial reduction in the volume of its expression, relative to the total volume of the limb bud, through these stages of

development. *Tbx2* expression shows a slightly different pattern where it is expressed most ubiquitously at stage 21 and then decreases by stage 24 but then increases slightly by stage 27.

The sharp boundary towards the centre of the limb of the posterior stripe of *Tbx3* expression may be maintained by some inhibitory factor/factors. Due to the clear complementary expression patterns of *Tbx3* and *Csal1* at stage 27 (Fig. 3.5, I.ii), *Csal1* may be a candidate for a transcription factor-encoding gene acting in this way.

3.3.2 Spalt genes

The most interesting change in *Csal1* expression throughout these stages is the shift between stage 24 and stage 27 where the expression changes from being completely at the distal tip of the limb bud with more posterior expression, to becoming proximally restricted and taking up a fairly central position in the limb. Mice with mutations in *Spalt* genes show defects in bone formation of the wrist. The region where *Csal1* is expressed in the stage 27 chick wing bud may correlate to the region that will later form the wrist joint. This would draw a parallel with the findings in *Sal1* mouse mutants where the phenotype includes wrist deformities and even some missing wrist elements (Kiefer et al., 2003). So Csal1 transcripts may first function in digit patterning in the early limb bud, and then have a second function later in limb development patterning the wrist.

Csal3 expression is detectable by stage 24, where it is expressed in the posterior and distal region of the limb but, unlike *Csal1* expression, it is completely dorsally restricted. By stage 27, this pattern has shifted and similarly to *Csal1* expression has moved away from the distal tip of the limb bud. Here it is also restricted to the posterior part of the limb bud and displays a cup-shaped pattern through the dorso-ventral axis.

Figure 3.7

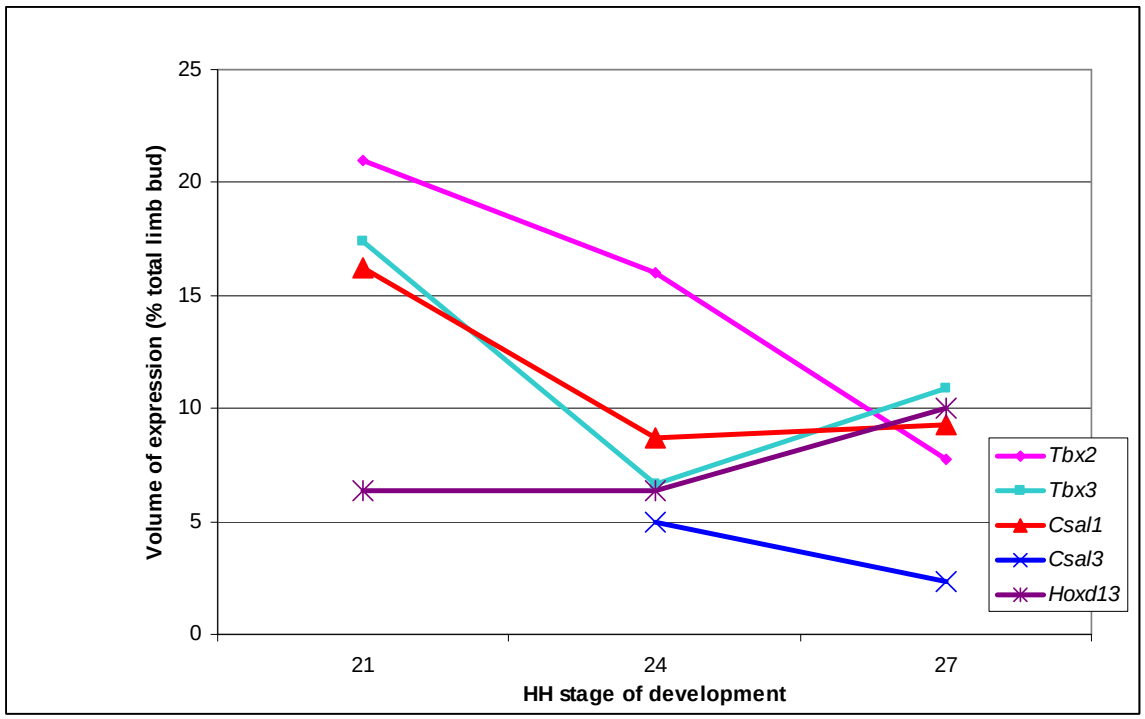
25
20
15
10
5
0
Volume of expression (% total limb bud)
21
24
27
HH stage of development
Tbx2
Tbx3
Csal1
Csal3
Hoxd13

Figure 3.7. Line graph showing changes in total median volume of expression patterns of transcription factor-encoding genes through three stages of development. Total volumes of gene expression patterns were calculated at each stage as a percentage of the whole reference limb bud. This allows for cross-comparison at different stages of development. The graph shows a general downward trend through time in the percentage of the limb bud showing expression of these genes although there is exception in the cases of *Tbx3* and *Csal1*, where the expression volume decreases and then increases slightly, and in *Hoxd13* where there is little change between the first two stages and then an increase by stage 27. It may be necessary to examine these expression patterns in more than 3 stages of development to gain a fuller understanding of how the expression changes through time.

Considering the changing volume of expression of *Spalt* genes through these stages, there is an overall decrease in the relative volumes of expression, although little change is observed in the latest two stages of *Csal1* expression.

3.3.3 *Hoxd13*

As mentioned in the introduction, expression of the *Hoxd* genes occurs with temporal and spatial co-linearity. However there is a deeper complexity to this type of expression in the developing limb bud because there are two phases of expression of these genes. During the first phase, genes *Hoxd9-13* are expressed sequentially where *Hoxd9* expression occurs in more of the limb than the other genes and *Hoxd13* is expressed most distally with the smallest expression pattern. During the next phase, which begins at around stage 22/23 (Nelson et al., 1996), the spatial co-linearity of the expression of *Hoxd9-13* is inverted where *Hoxd13* is the most ubiquitously expressed gene of this cluster. This correlates with my findings, where the relative volume of *Hoxd13* expression shows an overall increase through these three stages of development (Fig. 3.7). It is also known that as the limb bud expands, there is no initiation of *Hoxd13* expression in anterior, previously non-expressing cells (Vargesson et al., 1997), therefore this increase in volume of *Hoxd13* expressing cells is accountable only by proliferation and anterior migration of cells that already expressed this gene.

Conversely, other genes of the *Hoxd* cluster see a reduction in the volume of expression, which may be accounted for because cells of the expanding population in the posterior of the limb could switch off their expression of other *Hoxd* genes.

Chapter 4: Fate map of the chick wing bud using GFP chicken

4.1 Introduction

4.1.1 Fate mapping the developing limb

Fate mapping experiments have been carried out for many years and have contributed greatly to our understanding of developmental processes at a cellular level (Clarke and Tickle, 1999). The developing chick limb bud lends itself to these experiments due to the accessibility of the living embryo within the egg. An accurate fate map of the developing chick wing would be useful for determining the regions of the bud that go on to form specific structure. It could also be used to show how gene expressions in particular cell populations of the limb are maintained or altered through time.

There have been previous studies investigating cellular fate in the chick limb bud using various methods and aiming to answer a range of questions relating to limb development. A recent study by (Sato et al., 2007) used injection of lipophilic dyes, DiI and DiO to investigate how limb mesenchymal cells from the early limb bud become positioned along the PD axis. Their findings suggest that although there is some mixing of cells along this axis, it is apparent that cells that will go on to form proximal elements of the limb obtain their positional identity before those destined to form elements of more distal structures because results from spots of dye that were injected more proximally in the early limb bud were more consistent and did not spread out as much over time.

An earlier study used fate-mapping experiments to investigate AP patterning of the chick wing bud (Vargesson et al., 1997). The methods in this study also involved this

use of lipophilic dyes. This technique is advantageous in that it is non-invasive and the dyes can be applied fairly easily by injection. The dye labels the plasma membrane of up to 100 cells and the labelling continues to be detectable on cells that have divided from the original dyed population. Dilution does occur, however, and so cells can only be traced for up to 96 hours after injection. This means that cells can be traced from the very early limb bud to around the stage where small condensations of cells marking the digits can be detected. However, condensations which appear at this stage may later disappear as they mark digits which have been lost through natural selection (Welten et al., 2005), therefore interpretation of fate mapping using lipophilic dyes in relation to finding the precursor cells of extant digits may not be completely accurate. By injecting the stage 20 limb bud with spots of DiI and DiA at various positions, it was shown that cells of the distal, middle-to-posterior mesenchyme migrate anteriorly as well as distally as the limb bud expands.

Other previous methods of investigating cell fate in the chick limb have included applying small amounts of carbon or Indian ink onto the early limb bud. These methods are not extremely accurate but yet did provide basic information on the pattern of growth in the limb bud. Other methods include grafting of detectable cells such as those treated with tritiated thymidine (Stark and Searls, 1973) or tissue from quail embryos which can later be detected using stains specific to quail cell nuclei. In fact, it was use of this method that defined the origin of limb musculature (Chevallier et al., 1977).

This study represents the beginnings of an accurate, long term fate map of the chick wing bud using grafts from GFP-positive chick embryos, which have previously been used in fate mapping experiments of the avian tail bud (McGrew et al., 2008). This method of fate mapping of the limb, like previous methods, has various advantages and disadvantages; the main disadvantage being the invasiveness of grafting. The advantages are that the GFP-positive cells are easily and clearly detectable using a UV light source and as these cells divide among cells of the host embryo, their strength or detectability does not diminish over time. Thus the grafted embryos can be allowed to

develop to a stage where the skeletal elements of the limb are laid down in cartilage, and therefore the ability to deduce, with certainty, the fate of parts of the early limb bud with relation to the later skeleton and other specialised tissues. Another advantage of this technique is that the accuracy of the graft can be confirmed if the wing develops with normal patterning.

4.1.2 Formation of skeletal structures in the limb

During the development of skeletal structures in the limb, there are three main steps: commitment of cells to a chondrogenic lineage, condensation of these cells and then differentiation. Firstly, the cells of the mesenchyme separate into chondrogenic and non-chondrogenic domains. Subsequently, as differentiation begins, the physical beginnings of cartilage development become apparent, such as the production of an extra-cellular matrix and the appearance of major components of cartilage like aggrecan and type II collagen. These components are the foremost providers of structural integrity and strength in cartilage. The formation of cartilage can either act as a precursor to endochondral bone formation or can remain as cartilage, which is an important constituent of the skeleton. Cartilage also acts as a template for the production of the bone collar.

I have used two methods of identifying the extent of chondrogenesis in the chick wing. I have looked at differentiated cartilage using Alcian green staining and I have also looked at the expression patterns of the transcription factor-encoding gene *Sox9*. Alcian green is used to stain for cartilage. Specifically it detects glycosaminoglycans, which are a major component of cartilage. *Sox9* expression is among the most precocious markers of chondrogenesis in the limb (Akiyama, 2008), although it is important in various developmental processes throughout the body. Studies in chick have suggested that BMPs are required for maintenance of the expression of various *Sox* genes but the induction of *Sox9* occurs upstream of BMPs in the chondrogenic signalling cascade (Chimal-Monroy et al., 2003). It is present in humans, where along

with bone formation, it is required for development of the testis and heterozygous mutations in this gene are known to be the cause of campomelic dysplasia. This disorder is characterised by skeletal abnormalities throughout the body including curvature of bones in the legs and the development of a small chest cavity, which can sometimes result in death in newborns. In mouse, it has been demonstrated that osteo-chondroprogenitor cells are derived from *Sox9* expressing precursors (Akiyama et al., 2005) and ectopic expression of *Sox9* induces the expression of type II collagen (Bell et al., 1997). There is further evidence for a high level of conservation of the *Sox9* gene and its function as a precursor to chondrogenesis through vertebrate species, as this function has recently been identified in a member of the class Amphibia (Kerney and Hanken, 2008).

4.1.3 Aims of this chapter

The overall aim of this chapter is to gain insight into the normal development of the chick wing by observing the lineage of cells in 3D, through time in relation to the morphogenesis of defined structures, in particular the digits.

I aim to create a comprehensive, long-term fate map of the wing with tissue grafts using the GFP chicken. Specifically I aimed to define the populations of cells of the early limb bud which are progenitors of the digits, and then trace these cells during intermediate stages of development, equivalent to those at which I have gathered data on gene expression patterns. For completeness I also aim to record all of this fate map data in 3D, which will involve the use of indirect detection of GFP using in situ hybridization techniques described in chapter 2. To compare this to skeletogenesis in the limb, I also aim to record well-known markers for this in 3D.

4.2 Materials and methods

This section contains materials specific to this chapter on creating a fate map on the wing bud using the GFP chicken. For general materials and methods used throughout, see chapter 2.

4.2.1 GFP Chickens

GFP-positive transgenic chickens were created and supplied by the Transgenic Chicken Facility, Roslin Institute, Midlothian, UK (McGrew et al., 2004). The eggs are incubated in a 37ºC humidified incubator and are windowed in the same way as wild type eggs. On average, 50% of the eggs supplied are GFP-positive and these can easily be detected using a microscope with a UV light source.

4.2.2 Grafting

4.2.2.1 Preparation of the host

The eggs are windowed the day before grafting so that the membranes covering the embryo detach from the shell. This also allows for staging of the embryos and re-incubation to ensure that they are at a suitable stage for grafting.

Before any operations on the wing bud, the window of the shell is enlarged to an appropriate size by placing sellotape over the window and then using a small pair of scissors to cut a hole in the shell over the embryos. The two membranes (vitelline and amnion) that lie over the embryo must be torn away using a pair of fine forceps.

For fate mapping experiments by grafting, the segment of the limb bud that is removed should be exactly equivalent in shape, size and position in the limb bud to the piece of GFP-expressing tissue that will take its place. For this reason, the preparation of the host by removing a cube of the limb bud must be done accurately. The cuts are made using very small surgical scissors (Interfocus Ltd.) for the cuts perpendicular to the AER and fine needles for the cut parallel to the AER. This piece of tissue is then discarded.

4.2.2.2 Preparation of the graft

A GFP-expressing embryo of the same stage as the normal host embryo is dissected into PBS, where the membranes and head are removed. This embryo is the transferred to a small Petri dish with a few millimetres of solidified 1% agarose in the bottom of the dish and then filled with D-MEM containing Hepes (Invitrogen). Here the embryo can be pinned to the agarose using small dissecting pins, making it easier to cut out the graft. The first cut is made using small surgical scissors and the second is made using a fine needle. At this point the graft is impaled on a platinum pin. These are made using platinum wire (0.025mm diameter; Goodfellow metals), which is cut to the appropriate length and then bent into an L-shape. After impaling the graft, the final cut can be made using a fine needle, where the tissue is ready to be grafted.

4.2.2.3 Grafting the tissue

The graft is transferred to the host embryo using a miniature spatula. At first it is placed in a secure place such as on the embryo's body wall adjacent to the limb bud where it can be manoeuvred by gripping the hooked end of the pin with a pair of fine forceps and moving it to the prepared site. The pin is pressed securely into the host tissue. 1 drop of HEPES buffer (Invitrogen) containing 1% penicillin/streptomycin antibiotic is dropped onto the embryo. At this stage, the embryo is photographed twice, using a normal dissecting microscope with UV light source, *in ovo*: once under visible

light, and again under UV light. The photographs are taken in quick succession to minimise problems caused by the embryo moving slightly between photographs.

The grafted host embryo is re-incubated at 37°C until it reaches the desired stage. At this point the embryo is dissected and re-photographed in the same way as described above to visualise the fate of the grafted cells. These two photographs are overlaid using Adobe Photoshop™.

4.2.3 Analysis of grafted embryos

Once the final photographs of the grafted were taken, these were analysed simply by observation and with comparison to images of the wing skeleton at an equivalent stage. In cases where the wing developed abnormally (e.g. with too many or too few digits), it was considered that the original graft was flawed either in its position or in that the limb bud was damaged during the procedure. In these cases, the limbs were not analysed further.

4.2.4 Cloning of GFP gene

In order to carry out *in situ hybridization* experiments to detect the GFP protein expressed by tissue from the GFP chicken embryos, the GFP gene was cloned into a pGEM-T Easy vector before making an anti-sense RNA probe. Firstly, I designed oligonucleotide primers against the sequence for GFP. To do this I had the DNA containing GFP sequenced (sequencing service, Dundee University). I checked this sequence using the NCBI BLAST database to confirm that this was the correct gene. I designed oligonucleotides using a sequence complimentary to a 25 base pair strand at either end of the whole sequence.

To isolate and amplify this gene from a GFP containing plasmid (obtained from lab stocks), a PCR reaction was carried out. The mix included 2.5µl $MgCl_2$ (2.5mM), 5µl 10X buffer, 2.5µl dNTPs, 1µl taq polymerase, 1.5µl forward primer, 1.5µl reverse primer, 35µl dH_20 and 1µl plasmid DNA from maxi prep (diluted 1:200). I carried out electrophoresis on the amplification products using a 1.5% agarose gel, extracted using a Qiagen gel extraction kit and eluted in 35µl dH_20. 1µl of the DNA from this purification was ligated in a mix including 1µl of pGEM-T Easy vector, 0.5µl T4 DNA ligase, 5µl 2X ligation buffer, which was left overnight at 4°C. Top10 chemically competent *E. coli* cells (invitrogen) were transformed by thawing the cells on ice for 15 minutes, then adding 4µl of the ligation reaction. This was left on ice for 30 minutes, heat shocked at 65°C for 45 seconds and then left on ice for 15 minutes. The cells were then plated directly onto LB agar plates containing ampicillin (50µg/ml) and grown overnight at 37°C.

14 tubes, each with 4ml liquid LB containing ampicillin were inoculated with single colonies from the plate. To identify bacteria containing a plasmid with the cloned gene, a PCR was carried out where the mix contained 1µl bacterial culture, 31.5µl dH_20, 5µl $MgCl_2$, 5µl 5X buffer, 2.5µl dNTPs, 1µl Taq polymerase, 1.5µl of both M13 forward and reverse primers and 1µl formamide. By separating the DNA of the PCR product by electrophoresis, I found that one of the bacterial cultures contained the cloned gene. The DNA was extracted from the bacteria using a Qiagen mini prep kit, and which was then sequenced and confirmed to be the correct gene.

To make the probe using this plasmid, I followed the procedure as detailed in general materials and methods, using a PCR reaction to linerise the DNA and the transcription was carried out using SP6 RNA polymerase.

4.2.5 Alcian Green Staining for OPT

Embryos are fixed in 5% TCA (Trichloroacetic acid) overnight and then placed in 70% ethanol, 1% HCL for 2 hours. The embryos were stained in 1% Alcian Green in 70% ethanol, 1% HCL overnight and then dehydrated using 2 hour steps of successive ethanol concentrations (70%, 90% and 2 x 100%). If carrying out OPT on embryos, at this stage they are re-hydrated back to dH_20 in 2 hour steps of ethanol concentrations 90%, 70%, 50%, 25% and then in dH_20 for 2 hours. At this point the embryos are embedded and scanned following the normal OPT protocol.

4.3 Results

4.3.1 Fate map of 10 day wing

In order to create a long-term fate map, I replaced regions of the stage 21 wing bud with GFP-positive cells from the equivalent position around the margin of the limb bud. The initial position of the graft was recorded (see insets, Fig 4.1, B). These images were then superimposed onto a template of the wing bud to give the 7 different positions shown in Fig. 4.1. All grafts that were successfully carried out the specified positions gave the same result as shown (see n numbers, fig 4.1, B). In some cases, attempts at grafting at these positions were made where the outcome was the growth of a wing with abnormal patterning (e.g. an extra digit or missing digit). In these cases I assumed that the initial graft was inaccurate in some way or that the wing bud was damaged during the manipulation, so I have not included these in my results or in the "n" numbers in Figure 4.1. In all, 116 grafts were carried out and I have included 30 in my results. Note also that in some cases the grafted embryos did not survive to 10 days.

From observations of photographs of grafted embryos after 10 days and with comparison to images of the skeletal structures at this stage, I found that cells from position 1 at this anterior part in the wing bud (Fig 5.1, A) go to form the anterior part of the shoulder and also some connective tissue between the shoulder and wrist joints. The cells seem to have contributed to tissue lying adjacent, and anterior to radius. The fate of cells from the slightly posterior position 2 seems quite similar to that of cells from position 1 but without cells ending up in the shoulder joint and the strongest expression of GFP seems to be in a more distal position, closer to the wrist. There is, however, similar expression in the connective tissue between the shoulder and wrist anterior to the skeletal elements of the wing. Graft position 3 is more posterior than the previous two and just anterior to the midpoint of the wing bud. I have found that GFP-

positive cells grafted in this position form a stripe through the distal region of the developing radius, through the wrist and contribute to tissue of digit 2.

Position 4 involves cells at the midpoint of the AP axis in the stage 21 limb bud. Cells from this region go on to form a stripe similar to that formed by the cells from position 3, proximal to the wrist but more posterior. They are present in the wrist but rather than

contributing to digit 2, they appear in digit three and the surrounding tissue, extending to the very distal tip. Position 5 is more posterior still and cells from this cube of limb bud form a stripe in the tissue from the elbow to wrist along the posterior edge of this part of the limb. The cells are also present in the wrist and then extend in a thin stripe into the posterior border of the hand plate, where the stripe coincides with at least part of the region where digit 4 is forming. Position 6 involves cells slightly posterior to those in position 5, but part of these two regions is overlapping. Cells from this position contribute to a stripe from the elbow to wrist, similar to the stripe produced by grafting at position 5. The difference here is that no GFP-positive cells go into the hand plate. Position 7 is more posterior still and cells from here remain quite proximal, at the posterior edge of the elbow.

It is not always clear from these observations exactly which tissue the GFP expression appears in (e.g. skeleton or connective tissue). For more precise analysis, imaging using OPT or section *in situ* hybridization would be appropriate.

[figure 4.1]

Figure 4.1. Long term fate map of chick wing after 10 days of incubation. (A) Diagrammatic representation of the right chick wing bud at stage 21. Cubes labelled 1-7 represent sections of the limb bud that were replaced with GFP-positive tissue from wing buds of equivalent stage. Scale bar = 300μm. (B) Photographs of grafted wings after 10 days of incubation from a dorsal perspective. Insets show photographs of the wing bud immediately after grafting, where the outline of the wing bud and graft have been outlined for clarity. Cells from the grafts appear green. Numbers in bottom left of photographs and coloured borders relate to the graft positions marked in A. "n" numbers represent the number of grafts carried out at the same position. Scale bars = 1mm.

4.3.2 Fate map of the earlier chick wing bud

Now that I have identified the areas of the stage 21 wing bud that go on to form digits, it is possible to make a fate map to describe the position of the digit-forming cells at intervening stages of development. Fig 4.2 shows an embryo where a GFP graft was carried out at position 3 (see Fig 4.1), which will label cells that will form digit 2. The embryo was extracted from the egg 24 hours after grafting, at stage 26, and photographed. This shows how the cells of the graft have integrated into the limb and the way in which this region has expanded as the cells have divided. After photographing this embryo, I fixed it and carried out a normal whole mount *in situ* hybridization (detailed in section 2.3) to detect the GFP-positive cells with an RNA probe (Fig 4.2, C).

[figure 4.2]

Figure 4.2. Example of fate mapping of early chick wing bud. (A) Photograph of embryo *in ovo* immediately after grafting at stage 21. White line indicates outline of limb bud and graft. (B) Same embryo in (A) dissected 24 hours after grafting at Stage 26. Green shows GFP-expressing cells. (C) Whole mount *in situ* on same embryo to detect GFP. NTB:BCIP staining in same place as GFP expression in B.

4.3.3 3D markers of skeletal development in the Stage 27 wing bud

When the chick embryo reaches stage 27, the wing buds have become elongated and they begin to show external signs of where bony elements will begin to form. For example, Hamburger and Hamilton (1951) describe the beginnings of interdigital grooves on the dorsal surface. In order to investigate the extent of the development of bony elements in the wing bud at this stage, firstly I used alcian green staining. Alcian green is used to stain cartilage (the precursor to endochondral bone). I found that, at this stage, only the cartilage precursors to the humerus, radius and ulna are present. The digits are not yet laid down in cartilage. Alcian green patterns in the developing chick limb have previously been studied, although not in 3D in concert with gene expression patterns, as explored here.

Another method of distinguishing regions of cells that will go on to become bony elements is to examine areas of expression of the transcription factor encoding gene *Sox9*. *Sox9* is known to be expressed in chondroprogenitor cells in mouse embryogenesis and plays a role in chondrogenesis (Akiyama, 2008). Therefore the expression of *Sox9* is very transient. Here I show that in the stage 27 chick wing, *Sox9* is expressed in two distinct spots within the hand plate (Fig. 4.3, E). These spots correlate with the positions of digits 3 and 4 when they are formed at a slightly later stage. These findings are in keeping with *Sox9* expression patterns previously described at this stage (Welten et al., 2005).

I have mapped 3D images of both cartilage, stained using alcian green, and the expression pattern of *Sox9* to the reference limb at stage 27 (Fig 4.3, E). The patterns are understandably quite different but they each represent a useful framework when examining expression patterns of genes that are thought to be involved in shaping their development. I have shown, in figure 4.3(A-D), the three individual scans of alcian stained wings that have contributed to the median model of cartilage condensation at

this stage. The slight differences in these scans can be accounted for by the extremely dynamic nature of the process of bone formation. However, creating a median of these scans (4.3, D) gives us a reliable representation of the pattern of skeletal elements at this stage.

As described in section 3.2.3, by stage 27 of development, *Hoxd13* expression has spread towards the anterior margin of the distal wing bud. This area of expression represents the digit forming field and I have shown how this coincides with the expression of *Sox9* (4.3, F.i and ii).

[Figure 4.3]

Figure 4.3. Markers of early skeletal formation in the stage 27 wing bud. (A-D) 3D pattern of cartilage formation in the stage 27 wing bud. (A-C) Isosurface representations of OPT scans of stage 27 chick wing buds stained with alcian green and displayed in dorsal views (i) and in virtual sections (ii) with section positions marked by orange lines. (D) Median of scans A-C, indicated by white box. (E) Median pattern of cartilage formation (light grey) together with median *Sox9* expression. (F) Median *Sox9* expression together with *Hoxd13* expression as dorsal view (i) and virtual section (ii) where all *Sox9* expression is overlapped by *Hoxd13* expression.

4.4 Discussion

The fate map presented here is in reasonable agreement with previous fate mapping studies (Vargesson et al., 1997, Stark and Searls, 1973, Bowen et al., 1989), but these studies generally focus on different aspects of limb development than those addressed here. Some fate mapping experiments has previously been used to study the proximo-distal patterning of the limb, but I have attempted to distinguish the parts of the early limb bud that will form the digits and therefore my focus is on antero-posterior patterning. Previous attempts at this may have been hampered by the lack of a reliable and accurate technique. In a previous report (Vargesson et al., 1997), postulations were made on the origin of digits in the chick limb from injection of lipophilic dyes. In these experiments, the digits appear to come from positions slightly more posterior than those I have identified as digit forming positions. This difference, however, may be accounted for by the difference in stage of the initial manipulations, which in the paper by Vargesson et al., were carried out in stage 19/20 wing buds. This result may be expected due to the way in which Shh signalling expands the digit-forming field from stage 20 onwards (Towers et al., 2008). For completeness, it may be useful to do some more grafting experiments like this as a future study so that cells from the entire wing bud margin could be mapped, thus filling the gaps left between some of the positions described here.

I have shown the fate of blocks of tissue around the distal tip of the stage 21 chick wing bud and related this to the origin of the three digits of the chick wing. I have also shown the possibilities of using this technique to map the cells that will contribute to the digits at intermediate stages of development. The ability to use an antisense GFP probe for whole mount *in situ* hybridization to detect grafted cells creates new possibilities for visualising cell fate in the developing limb. This is not necessary for 2D visualisation because the green cells are visible with use of a UV light source. However, when carrying out OPT on these samples, I have found that without

previously detecting the GFP-positive cells with an RNA probe, it is not possible to distinguish between normal tissue and grafted tissue. The washes, dehydration and clearing with BABB prior to OPT are enough to dissipate the GFP-expression.

I have also shown markers for skeletal structure development in the chick wing in 3D, which could be combined with a 3D fate map to derive information on the origin of cells contributing to skeletal structures.

Chapter 5: General Conclusions

Here I have mapped 3D expression patterns of transcription factor-encoding genes involved in digit development to reference limbs at three different stages of development. This allowed me to compare and analyse the expression patterns both spatially and temporally. Investigating the same gene expression patterns at three different stages of development allowed for appreciation of their dynamism.

I have also created a long-term fate map of the chick wing and from this I established which cell populations from the early bud contribute to the digits. I have added to this 3D data on well-known markers of skeletogenesis to allow relation of gene expression patterns and fate map to limb morphogenesis.

This work shows some of the possibilities that are now available to accumulate gene expression and tissue anatomy in 3D, and also how this could be combined with a 3D fate map. Therefore, these techniques could be built upon to describe expression patterns not only in 3D but through time in relation to the appearance of specialised tissue.

One specific question I have aimed to address relates to the way in which digits gain their identity. By integrating fate mapping and gene expression studies as shown here, it would be possible to determine exactly which genes are expressed in the limb bud tissue destined to become digits and further experiments could help to establish whether this combination of gene expression through time instructs the digit on its identity.

As this work will go towards the larger project aimed at producing an atlas of gene expression in the chick embryo (see section 1.2), clearly there will be a great deal of future work in this area using methods similar to those used here to map the expression patterns of thousands of genes. This work will be continued in the immediate future to

map many other gene expression patterns in the chick wing to the reference at stage 24. By focussing on one particular stage, it will be possible to quickly map many gene expression patterns and with more patterns at the same stage comes greater opportunity for computational analysis. Another focus for the immediate future is to map the expression of *Shh* through the time course of its activity, due to its importance as a limb patterning gene. This would act as a useful reference point when studying other gene expression patterns.

To combine the fate map with gene expression, as described above, it will be essential to carry out more fate mapping experiments concentrating on the regions of the limb bud that contribute to digits. These fate maps will be recorded in 3D at the 3 stages where information on gene expression patterns is available in order to make comparisons.

Similarly to the way I have shown markers for skeletal formation in the wing bud in 3D, it would be possible to use antibody staining or to carry out whole mount *in situ* hybridization experiments to detect precursor cells of other types of tissue present in the limb. For example, muscle and tendon tissue could be mapped in 3D and added to a model of the limb by mapping. This would be complimentary to the recent publication of such 3D data in the mouse limb (Delaurier et al., 2008).

Overall, recent technological advances have created more possibilities in relation to the description of embryonic development. There has also been a fairly recent switch to the availability of online reference databases as aids to research. Considering these two factors, the work presented here shows how the study of development can benefit from the use of new technology.

References

Akiyama, H. (2008) Control of chondrogenesis by the transcription factor Sox9. *Mod Rheumatol,* 18**,** 213-9.

Akiyama, H., Kamitani, T., Yang, X., Kandyil, R., Bridgewater, L. C., Fellous, M., Mori-Akiyama, Y. & De Crombrugghe, B. (2005) The transcription factor Sox9 is degraded by the ubiquitin-proteasome system and stabilized by a mutation in a ubiquitin-target site. *Matrix Biol,* 23**,** 499-505.

Baldock, R. A., Bard, J. B., Burger, A., Burton, N., Christiansen, J., Feng, G., Hill, B., Houghton, D., Kaufman, M., Rao, J., Sharpe, J., Ross, A., Stevenson, P., Venkataraman, S., Waterhouse, A., Yang, Y. & Davidson, D. R. (2003) EMAP and EMAGE: a framework for understanding spatially organized data. *Neuroinformatics,* 1**,** 309-25.

Bamshad, M., Le, T., Watkins, W. S., Dixon, M. E., Kramer, B. E., Roeder, A. D., Carey, J. C., Root, S., Schinzel, A., Van Maldergem, L., Gardner, R. J., Lin, R. C., Seidman, C. E., Seidman, J. G., Wallerstein, R., Moran, E., Sutphen, R., Campbell, C. E. & Jorde, L. B. (1999) The spectrum of mutations in TBX3: Genotype/Phenotype relationship in ulnar-mammary syndrome. *Am J Hum Genet,* 64**,** 1550-62.

Bamshad, M., Lin, R. C., Law, D. J., Watkins, W. C., Krakowiak, P. A., Moore, M. E., Franceschini, P., Lala, R., Holmes, L. B., Gebuhr, T. C., Bruneau, B. G., Schinzel, A., Seidman, J. G., Seidman, C. E. & Jorde, L. B. (1997) Mutations in human TBX3 alter limb, apocrine and genital development in ulnar-mammary syndrome. *Nat Genet,* 16**,** 311-5.

Barrio, R., Shea, M. J., Carulli, J., Lipkow, K., Gaul, U., Frommer, G., Schuh, R., Jackle, H., Kafatos, F. C. (1996) The *spalt-related* gene of *Drosophila melanogaster* is a member of an ancient gene family, defined by the adjacent, region-specific homeotic gene *spalt*. *Development Genes and Evolution,* 206**,** 315.

Bell, D. M., Leung, K. K., Wheatley, S. C., Ng, L. J., Zhou, S., Ling, K. W., Sham, M. H., Koopman, P., Tam, P. P. & Cheah, K. S. (1997) SOX9 directly regulates the type-II collagen gene. *Nat Genet,* 16**,** 174-8.

Bell, G. W., Yatskievych, T. A. & Antin, P. B. (2004) GEISHA, a whole-mount in situ hybridization gene expression screen in chicken embryos. *Dev Dyn,* 229**,** 677-87.

Biehs, B., Sturtevant, M. A. & Bier, E. (1998) Boundaries in the Drosophila wing imaginal disc organize vein-specific genetic programs. *Development,* 125**,** 4245-57.

Biesecker, L. G. (2008) The Greig cephalopolysyndactyly syndrome. *Orphanet J Rare Dis,* 3**,** 10.

Bookstein, F. L. (1989) Principal Warps - Thin-Plate Splines and the Decomposition of Deformations. *Ieee Transactions on Pattern Analysis and Machine Intelligence,* 11**,** 567-585.

Bowen, J., Hinchliffe, J. R., Horder, T. J. & Reeve, A. M. (1989) The fate map of the chick forelimb-bud and its bearing on hypothesized developmental control mechanisms. *Anat Embryol (Berl),* 179**,** 269-83.

Bridges, C. B. & Morgan, T. H. (1923) *The Third Chromosome Group of Mutant Characters of Drosophila Melanogaster*, Washington, Carnegie Institute of Washington.

Brown, W. R., Hubbard, S. J., Tickle, C. & Wilson, S. A. (2003) The chicken as a model for large-scale analysis of vertebrate gene function. *Nat Rev Genet,* 4**,** 87-98.

Chen, C. K., Kuhnlein, R. P., Eulenberg, K. G., Vincent, S., Affolter, M. & Schuh, R. (1998) The transcription factors KNIRPS and KNIRPS RELATED control cell migration and branch morphogenesis during Drosophila tracheal development. *Development,* 125**,** 4959-68.

Chevallier, A., Kieny, M. & Mauger, A. (1977) Limb-somite relationship: origin of the limb musculature. *J Embryol Exp Morphol,* 41**,** 245-58.

Chiang, C., Litingtung, Y., Lee, E., Young, K. E., Corden, J. L., Westphal, H. & Beachy, P. A. (1996) Cyclopia and defective axial patterning in mice lacking Sonic hedgehog gene function. *Nature,* 383**,** 407-13.

Chimal-Monroy, J., Rodriguez-Leon, J., Montero, J. A., Ganan, Y., Macias, D., Merino, R. & Hurle, J. M. (2003) Analysis of the molecular cascade responsible for mesodermal limb chondrogenesis: Sox genes and BMP signaling. *Dev Biol,* 257**,** 292-301.

Christiansen, J. H., Yang, Y., Venkataraman, S., Richardson, L., Stevenson, P., Burton, N., Baldock, R. A. & Davidson, D. R. (2006) EMAGE: a spatial database of gene expression patterns during mouse embryo development. *Nucleic Acids Res,* 34**,** D637-41.

Chudek, J. A., Hunter, G., Sprent, J. I. & Wurz, G. (1997) An application of NMR microimaging to investigate nitrogen fixing root nodules. *Magn Reson Imaging,* 15**,** 361-8.

Clarke, J. D. & Tickle, C. (1999) Fate maps old and new. *Nat Cell Biol,* 1**,** E103-9.

Cohn, M. J. (2000) Developmental biology. Giving limbs a hand. *Nature,* 406**,** 953-4.

Davenport, T. G., Jerome-Majewska, L. A. & Papaioannou, V. E. (2003) Mammary gland, limb and yolk sac defects in mice lacking Tbx3, the gene mutated in human ulnar mammary syndrome. *Development,* 130**,** 2263-73.

De Celis, J. F., Barrio, R. & Kafatos, F. C. (1996) A gene complex acting downstream of dpp in Drosophila wing morphogenesis. *Nature,* 381**,** 421-4.

Delaurier, A., Burton, N., Bennett, M., Baldock, R., Davidson, D., Mohun, T. J. & Logan, M. P. (2008) The Mouse Limb Anatomy Atlas: an interactive 3D tool for studying embryonic limb patterning. *BMC Dev Biol,* 8**,** 83.

Dolle, P., Dierich, A., Lemeur, M., Schimmang, T., Schuhbaur, B., Chambon, P. & Duboule, D. (1993) Disruption of the Hoxd-13 gene induces localized heterochrony leading to mice with neotenic limbs. *Cell,* 75**,** 431-41.

Drossopoulou, G., Lewis, K. E., Sanz-Ezquerro, J. J., Nikbakht, N., Mcmahon, A. P., Hofmann, C. & Tickle, C. (2000) A model for anteroposterior patterning of the vertebrate limb based on sequential long- and short-range Shh signalling and Bmp signalling. *Development,* 127**,** 1337-48.

Farrell, E. R. & Munsterberg, A. E. (2000) csal1 is controlled by a combination of FGF and Wnt signals in developing limb buds. *Dev Biol,* 225**,** 447-58.

Fisher, M. E., Clelland, A. K., Bain, A., Baldock, R. A., Murphy, P., Downie, H., Tickle, C., Davidson, D. R. & Buckland, R. A. (2008) Integrating technologies for comparing 3D gene expression domains in the developing chick limb. *Dev Biol,* 317**,** 13-23.

Fromental-Ramain, C., Warot, X., Messadecq, N., Lemeur, M., Dolle, P. & Chambon, P. (1996) Hoxa-13 and Hoxd-13 play a crucial role in the patterning of the limb autopod. *Development,* 122**,** 2997-3011.

Gibson-Brown, J. J., Agulnik, S. I., Silver, L. M., Niswander, L. & Papaioannou, V. E. (1998) Involvement of T-box genes Tbx2-Tbx5 in vertebrate limb specification and development. *Development,* 125**,** 2499-509.

Graham, A., Papalopulu, N. & Krumlauf, R. (1989) The murine and Drosophila homeobox gene complexes have common features of organization and expression. *Cell,* 57**,** 367-78.

Hamburger, V. & Hamilton, H. (1951) A series of normal stages in the development of the chick embryo. *Journal of Morphology,* 88.

Harfe, B. D., Scherz, P. J., Nissim, S., Tian, H., Mcmahon, A. P. & Tabin, C. J. (2004) Evidence for an expansion-based temporal Shh gradient in specifying vertebrate digit identities. *Cell,* 118**,** 517-28.

Isaac, A., Rodriguez-Esteban, C., Ryan, A., Altabef, M., Tsukui, T., Patel, K., Tickle, C. & Izpisua-Belmonte, J. C. (1998) Tbx genes and limb identity in chick embryo development. *Development,* 125**,** 1867-75.

Kerney, R. & Hanken, J. (2008) Gene expression reveals unique skeletal patterning in the limb of the direct-developing frog, Eleutherodactylus coqui. *Evol Dev,* 10**,** 439-48.

Kiefer, S. M., Ohlemiller, K. K., Yang, J., Mcdill, B. W., Kohlhase, J. & Rauchman, M. (2003) Expression of a truncated Sall1 transcriptional repressor is responsible for Townes-Brocks syndrome birth defects. *Hum Mol Genet,* 12**,** 2221-7.

Kohlhase, J., Wischermann, A., Reichenbach, H., Froster, U. & Engel, W. (1998) Mutations in the SALL1 putative transcription factor gene cause Townes-Brocks syndrome. *Nat Genet,* 18**,** 81-3.

Koster, R., Stick, R., Loosli, F. & Wittbrodt, J. (1997) Medaka spalt acts as a target gene of hedgehog signaling. *Development,* 124**,** 3147-56.

Laufer, E., Nelson, C. E., Johnson, R. L., Morgan, B. A. & Tabin, C. (1994) Sonic hedgehog and Fgf-4 act through a signaling cascade and feedback loop to integrate growth and patterning of the developing limb bud. *Cell,* 79**,** 993-1003.

Lein, E. S., Hawrylycz, M. J., Ao, N., Ayres, M., Bensinger, A., Bernard, A., Boe, A. F., Boguski, M. S., Brockway, K. S., Byrnes, E. J., Chen, L., Chen, T. M., Chin, M. C., Chong, J., Crook, B. E., Czaplinska, A., Dang, C. N., Datta, S., Dee, N. R., Desaki, A. L., Desta, T., Diep, E., Dolbeare, T. A., Donelan, M. J., Dong, H. W., Dougherty, J. G., Duncan, B. J., Ebbert, A. J., Eichele, G., Estin, L. K., Faber, C., Facer, B. A., Fields, R., Fischer, S. R., Fliss, T. P., Frensley, C., Gates, S. N., Glattfelder, K. J., Halverson, K. R., Hart, M. R., Hohmann, J. G., Howell, M. P., Jeung, D. P., Johnson, R. A., Karr, P. T., Kawal, R., Kidney, J. M., Knapik, R. H., Kuan, C. L., Lake, J. H., Laramee, A. R., Larsen, K. D., Lau, C., Lemon, T. A., Liang, A. J., Liu, Y., Luong, L. T., Michaels, J., Morgan, J. J., Morgan, R. J., Mortrud, M. T., Mosqueda, N. F., Ng, L. L., Ng, R., Orta, G. J., Overly, C. C., Pak, T. H., Parry, S. E., Pathak, S. D., Pearson, O. C., Puchalski, R. B., Riley, Z. L., Rockett, H. R., Rowland, S. A., Royall, J. J., Ruiz, M. J., Sarno, N. R., Schaffnit, K., Shapovalova, N. V., Sivisay, T., Slaughterbeck, C. R., Smith, S. C., Smith, K. A., Smith, B. I., Sodt, A. J., Stewart, N. N., Stumpf, K. R., Sunkin, S. M., Sutram, M., Tam, A., Teemer, C. D., Thaller, C., Thompson, C. L., Varnam, L. R., Visel, A., Whitlock, R. M., Wohnoutka, P. E., Wolkey, C. K., Wong, V. Y., Wood, M., et al. (2007) Genome-wide atlas of gene expression in the adult mouse brain. *Nature,* 445**,** 168-76.

Li, X., Liu, J., Davey, M., Duce, S., Jaberi, N., Liu, G., Davidson, G., Tenent, S., Mahood, R., Brown, P., Cunningham, C., Bain, A., Beattie, K., Mcdonald, L., Schmidt, K., Towers, M., Tickle, C. & Chudek, S. (2007) Micro-magnetic resonance imaging of avian embryos. *J Anat,* 211**,** 798-809.

Logan, M., Simon, H. G. & Tabin, C. (1998) Differential regulation of T-box and homeobox transcription factors suggests roles in controlling chick limb-type identity. *Development,* 125**,** 2825-35.

Maniatis, T., Fritsch, E. & Sambrook, J. (1982) *Molecular Cloning: A Laboratory Manual.,* New York, Cold Springs Harbor Press.

Marigo, V., Davey, R. A., Zuo, Y., Cunningham, J. M. & Tabin, C. J. (1996) Biochemical evidence that patched is the Hedgehog receptor. *Nature,* 384**,** 176-9.

Mcgrew, M. J., Sherman, A., Ellard, F. M., Lillico, S. G., Gilhooley, H. J., Kingsman, A. J., Mitrophanous, K. A. & Sang, H. (2004) Efficient production of germline transgenic chickens using lentiviral vectors. *EMBO Rep,* 5**,** 728-33.

Mcgrew, M. J., Sherman, A., Lillico, S. G., Ellard, F. M., Radcliffe, P. A., Gilhooley, H. J., Mitrophanous, K. A., Cambray, N., Wilson, V. & Sang, H. (2008) Localised axial progenitor cell populations in the avian tail bud are not committed to a posterior Hox identity. *Development,* 135**,** 2289-99.

Nelson, C. E., Morgan, B. A., Burke, A. C., Laufer, E., Dimambro, E., Murtaugh, L. C., Gonzales, E., Tessarollo, L., Parada, L. F. & Tabin, C. (1996) Analysis of Hox gene expression in the chick limb bud. *Development,* 122**,** 1449-66.

Nissim, S., Allard, P., Bandyopadhyay, A., Harfe, B. D. & Tabin, C. J. (2007) Characterization of a novel ectodermal signaling center regulating Tbx2 and Shh in the vertebrate limb. *Dev Biol,* 304**,** 9-21.

Niswander, L., Jeffrey, S., Martin, G. R. & Tickle, C. (1994) A positive feedback loop coordinates growth and patterning in the vertebrate limb. *Nature,* 371**,** 609-12.

Niswander, L., Tickle, C., Vogel, A., Booth, I. & Martin, G. R. (1993) FGF-4 replaces the apical ectodermal ridge and directs outgrowth and patterning of the limb. *Cell,* 75**,** 579-87.

Pflugfelder, G. O., Roth, H., Poeck, B., Kerscher, S., Schwarz, H., Jonschker, B. & Heisenberg, M. (1992) The lethal(1)optomotor-blind gene of Drosophila melanogaster is a major organizer of optic lobe development: isolation and characterization of the gene. *Proc Natl Acad Sci U S A,* 89**,** 1199-203.

Riddle, R. D., Johnson, R. L., Laufer, E. & Tabin, C. (1993) Sonic hedgehog mediates the polarizing activity of the ZPA. *Cell,* 75**,** 1401-16.

Ros, M. A., Dahn, R. D., Fernandez-Teran, M., Rashka, K., Caruccio, N. C., Hasso, S. M., Bitgood, J. J., Lancman, J. J. & Fallon, J. F. (2003) The chick oligozeugodactyly (ozd) mutant lacks sonic hedgehog function in the limb. *Development,* 130**,** 527-37.

Ruiz I Altaba, A. (1999) The works of GLI and the power of hedgehog. *Nat Cell Biol,* 1**,** E147-8.

Sato, K., Koizumi, Y., Takahashi, M., Kuroiwa, A. & Tamura, K. (2007) Specification of cell fate along the proximal-distal axis in the developing chick limb bud. *Development,* 134**,** 1397-406.

Saunders, J. W., Jr. & Gasseling, M. T. (1968) Ectoderm-mesenchymal interaction in the origins of wing symetry. *In epithelial-mesenchymal interactions, R. Fleischmajer and R. E. Billingham Eds. (Baltimore: Williams and Wilkins)***,** 19.

Sharpe, J. (2002) 12 New approaches for studying limb development: optical projection tomography and computer modelling. *J Anat,* 201**,** 420.

Sharpe, J., Ahlgren, U., Perry, P., Hill, B., Ross, A., Hecksher-Sorensen, J., Baldock, R. & Davidson, D. (2002) Optical projection tomography as a tool for 3D microscopy and gene expression studies. *Science,* 296**,** 541-5.

Shen, J., Dorner, C., Bahlo, A. & Pflugfelder, G. O. (2008) optomotor-blind suppresses instability at the A/P compartment boundary of the Drosophila wing. *Mech Dev,* 125**,** 233-46.

Shin, S. H., Kogerman, P., Lindstrom, E., Toftgard, R. & Biesecker, L. G. (1999) GLI3 mutations in human disorders mimic Drosophila cubitus interruptus protein functions and localization. *Proc Natl Acad Sci U S A,* 96**,** 2880-4.

Stark, R. J. & Searls, R. L. (1973) A description of chick wing bud development and a model of limb morphogenesis. *Dev Biol,* 33**,** 138-53.

Stone, D. M., Hynes, M., Armanini, M., Swanson, T. A., Gu, Q., Johnson, R. L., Scott, M. P., Pennica, D., Goddard, A., Phillips, H., Noll, M., Hooper, J. E., De Sauvage, F. & Rosenthal, A. (1996) The tumour-suppressor gene patched encodes a candidate receptor for Sonic hedgehog. *Nature,* 384**,** 129-34.

Sturtevant, M. A., Biehs, B., Marin, E. & Bier, E. (1997) The spalt gene links the A/P compartment boundary to a linear adult structure in the Drosophila wing. *Development,* 124**,** 21-32.

Summerbell, D. (1974) Interaction between the proximo-distal and antero-posterior co-ordinates of positional value during the specification of positional information in the early development of the chick limb-bud. *J Embryol Exp Morphol,* 32**,** 227-37.

Summerhurst, K., Stark, M., Sharpe, J., Davidson, D. & Murphy, P. (2008) 3D representation of Wnt and Frizzled gene expression patterns in the mouse embryo at embryonic day 11.5 (Ts19). *Gene Expr Patterns,* 8**,** 331-48.

Suzuki, T., Takeuchi, J., Koshiba-Takeuchi, K. & Ogura, T. (2004) Tbx Genes Specify Posterior Digit Identity through Shh and BMP Signaling. *Dev Cell,* 6**,** 43-53.

Sweetman, D., Smith, T., Farrell, E. R., Chantry, A. & Munsterberg, A. (2003) The conserved glutamine-rich region of chick csal1 and csal3 mediates protein interactions with other spalt family members. Implications for Townes-Brocks syndrome. *J Biol Chem,* 278**,** 6560-6.

Sweetman, D., Smith, T. G., Farrell, E. R. & Munsterberg, A. (2005) Expression of csal1 in pre limb-bud chick embryos. *Int J Dev Biol,* 49**,** 427-30.

Tarchini, B., Duboule, D. & Kmita, M. (2006) Regulatory constraints in the evolution of the tetrapod limb anterior-posterior polarity. *Nature,* 443**,** 985-8.

Tickle, C., Shellswell, G., Crawley, A. & Wolpert, L. (1976) Positional signalling by mouse limb polarising region in the chick wing bud. *Nature,* 259**,** 396-7.

Tickle, C., Summerbell, D. & Wolpert, L. (1975) Positional signalling and specification of digits in chick limb morphogenesis. *Nature,* 254**,** 199-202.

Towers, M., Mahood, R., Yin, Y. & Tickle, C. (2008) Integration of growth and specification in chick wing digit-patterning. *Nature,* 452**,** 882-6.

Tumpel, S., Sanz-Ezquerro, J. J., Isaac, A., Eblaghie, M. C., Dobson, J. & Tickle, C. (2002) Regulation of Tbx3 expression by anteroposterior signalling in vertebrate limb development. *Dev Biol,* 250**,** 251-62.

Vargesson, N., Clarke, J. D., Vincent, K., Coles, C., Wolpert, L. & Tickle, C. (1997) Cell fate in the chick limb bud and relationship to gene expression. *Development,* 124**,** 1909-18.

Vokes, S. A., Ji, H., Wong, W. H. & Mcmahon, A. P. (2008) A genome-scale analysis of the cis-regulatory circuitry underlying sonic hedgehog-mediated patterning of the mammalian limb. *Genes Dev,* 22**,** 2651-63.

Wallis, J. W., Aerts, J., Groenen, M. A., Crooijmans, R. P., Layman, D., Graves, T. A., Scheer, D. E., Kremitzki, C., Fedele, M. J., Mudd, N. K., Cardenas, M., Higginbotham, J., Carter, J., Mcgrane, R., Gaige, T., Mead, K., Walker, J., Albracht, D., Davito, J., Yang, S. P., Leong, S., Chinwalla, A., Sekhon, M., Wylie, K., Dodgson, J., Romanov, M. N., Cheng, H., De Jong, P. J., Osoegawa, K., Nefedov, M., Zhang, H., Mcpherson, J. D., Krzywinski, M., Schein, J., Hillier, L., Mardis, E. R., Wilson, R. K. & Warren, W. C. (2004) A physical map of the chicken genome. *Nature,* 432**,** 761-4.

Wang, B., Fallon, J. F. & Beachy, P. A. (2000) Hedgehog-regulated processing of Gli3 produces an anterior/posterior repressor gradient in the developing vertebrate limb. *Cell,* 100**,** 423-34.

Wellik, D. M. & Capecchi, M. R. (2003) Hox10 and Hox11 genes are required to globally pattern the mammalian skeleton. *Science,* 301**,** 363-7.

Welten, M. C., Verbeek, F. J., Meijer, A. H. & Richardson, M. K. (2005) Gene expression and digit homology in the chicken embryo wing. *Evol Dev,* 7**,** 18-28.

Zakany, J., Kmita, M. & Duboule, D. (2004) A dual role for Hox genes in limb anterior-posterior asymmetry. *Science,* 304**,** 1669-72.

Zhu, J., Nakamura, E., Nguyen, M. T., Bao, X., Akiyama, H. & Mackem, S. (2008) Uncoupling Sonic hedgehog control of pattern and expansion of the developing limb bud. *Dev Cell,* 14**,** 624-32.

Appendix 1

Supplementary Figures

Movie 1

Expression patterns of transcription factor-encoding genes in the stage 21 chick wing bud. In order of appearance, first limb bud anatomy, and expression patterns shown are of genes *Tbx3* (pink), *Tbx2* (green), *Hoxd13* (purple), *Csal1* (red).

Movie 2

Expression patterns of transcription factor-encoding genes in the stage 24 chick wing bud. In order of appearance, first limb bud anatomy, and expression patterns shown are of genes *Tbx3* (pink), *Tbx2* (green), *Hoxd13* (purple), *Csal1* (red), *Csal3* (blue).

Movie 3

Expression patterns of transcription factor-encoding genes and Alcian Green staining in the stage 27 chick wing bud. In order of appearance, first limb bud anatomy, Alcian Green staining (light grey), *Tbx3* (pink), *Tbx2* (green), *Csal3* (blue), *Csal1* (red), *Hoxd13* (purple).

[figure 4]

Supplementary figure 4. Shh signalling pathway. (A) In the absence of Shh ligand, Smoothened is inhibited by Patched. This inhibition activates a transcriptional repressor of Gli (B) In the presence of Shh ligand, Smoothened is no longer inhibited and Gli proteins can then enter the cell nucleus where they act as transcriptional activators.

Appendix 2

Recipes

Hybridization buffer

50% Formamide (Fisher)
5xSSC
2% Blocking buffer (Roche)
0.1% Triton-X100 (Sigma)
0.1% CHAPS (Fisher)
20µg/ml tRNA (Boehringer)
5mM EDTA (Sigma)
50µg/ml Heparin (Sigma)

Phosphate buffered saline (PBS)

PBS was diluted from a 10X stock solution, made up using 10X phosphate buffered saline powder (Fisher Scientific). 1L of PBS was treated with 1ml diethyl pyrocarbonate (DEPC) (Sigma) overnight and then autoclaved.

Phosphate buffered saline + Tween20 (PBT)

PBT was made by adding 1ml of Tween-20 (Sigma) to 1L of DEPC treated PBS.

Tris Buffered saline + Tween20 (TBST)

50mM Tris-Cl (Sigma) pH7.5

150mM NaCl (Sigma)

0.1% Tween-20 (Sigma)

Maleic acid buffer + Tween20 (MABT)

100 mM Maleic acid

150mM NaCl

0.1% Tween-20

pH7.5

20X SSC (1L)

175.3g NaCl

88.2g sodium citrate

1L dH_20

NTMT

100 mM Tris-HCl (Sigma) pH9.5

50mM MgCl (Sigma)

100mM NaCl (Sigma)

0.1% Tween-20 (Sigma)